29th Canadian Tectonics Group Workshop

Co-hosted by the Structural Geology and Tectonics Division of the Geological Association of Canada

October 2-4, 2009

Manitou Lodge, Pine Falls, Manitoba

Program with Abstracts

Fieldtrip Guide

Schedule of Events 29th Canadian Tectonics Group Workshop
Pine Falls, Manitoba and Rice Lake Greenstone Belt

Friday, October 2nd

18:00 – 23:00 Welcome to the 2009 Canadian Tectonics Group Workshop
Registration, Ice Breaker and poster set up

Saturday, October 3rd

Rice Lake greenstone belt field trip

07:00 – 08:00 Breakfast at Papertown Inn

08:00 – 09:30 Drive to Bissett

09:00 – 09:10 Opening remarks and safety briefing: Scott Anderson

09:10 – 12:00 Stop 1: Bidou assemblage, Rainy Lake Road unit
Stop 2: Bidou assemblage, Rainy Lake Road unit
Stop 3: Bidou assemblage, Round Lake unit
Stop 4: Bidou assemblage, Round Lake unit

12:00 – 12:30 Lunch

12:30 – 17:00 Stop 5: San Antonio assemblage, basal unconformity
Stop 6: San Antonio assemblage, Gold Creek syncline
Stop 7: San Antonio assemblage, Horseshoe Lake anticline
Stop 8: San Antonio assemblage, Wanipigow Shear zone

17:00 – 18:30 Drive to Pine Falls

18:30 – 19:30 Dinner

19:30 – 20:30 Annual GAC/SGTD meeting

Sunday, October 4th

Technical Session

The program presents the schedule of oral and poster presentations. Oral presentations are 20 minutes long, with 5 minutes for questions.

07:00 – 09:00 Breakfast, Papertown Inn

09:00 – 09:05 Introductory remarks: Chris Beaumont-Smith

09:05 – 09:30 **Sharon Carr and Phillip Simony**
Criteria for evaluating channel flow in ancient orogens, and an example from the SE Canadian Cordillera in support of Couette (transport) rather than Poiseulle (channel) flow

9:30 – 09:55 **Richard Bailey and C. Robin**
Diapirism and the early generation of continental crust

09:55 – 10:20 **Lori Kennedy, Kelly Russell and E. Nelles**
Residual porosity as an explanation for ductile-brittle behaviour during dome extrusion: experimental constraints

10:20 – 10:45 Poster presentations and coffee break

10:45 – 11:10 **Willem Langenberg**
LiDAR, GIS and down-plunge cross sections

11:10 – 11:35 **Kelly Russell, S. Quane and G. Andrews**
Timescales of compaction in volcanic systems

11:35 – 13:00 Lunch at Papertown Inn

13:00 – 13:25 **Changcheng Li and Dahzi Jaing**
Fold evolution and development of mylonites in the Grenville Front Tectonic Zone southeast of Sudbury, Ontario, Canada

13:25 – 13:50 **Fried Schwerdtner, , S Lu, J. Yang and D. Landa**
Investigating the evolution of the Big Turn, Grenville Orogen of central Ontario: progress report

13:50 – 14:15 **Jurgen Kraus**
A fractured gas reservoir in a composite foreland basin, Sichuan Province, China

14:30 – 16:00 Drive to Winnipeg Airport

Posters

Chris Beaumont-Smith
Structural geology and gold metallogeny of the New Britannia mine area, Snow Lake, Manitoba

Benjamin Stanley, Shoufa Lin and Cees van Staal
Structural geology of the Kluane Metamorphic Assemblage, southwest Yukon Territory, Canada

Diapirism and the early generation of continental crust

Bailey, R.C. and Robin, C.

University of Toronto, Toronto, ON M5S 3B1

We will review recent numerical modelling work which suggests that Hadean and paleo-Archean diapiric overturn of submarine mafic volcanics into the lower crust was rapid enough to act as the mechanical engine for the production of early felsic continental crust, by deep remelting of mafic metavolcanics. Put another way, whether or not plate tectonics operated during the Archean, it may not have been necessary for the production of continental crust. These numerical models describe both overall structure and detailed strain history which can be compared with field observations. However, comparisons with field data face two important obstacles. First, field observations record the last (and perhaps atypical) stages of such Archean diapirism, that which was frozen to a halt as the enabling conditions ceased, and second, granitoid melting (which may be a late feature) is not incorporated in the models. These models may therefore be applicable mostly to Hadean and neo-Archean processes which are not well preserved. The numerical model as such provides no insight into the "granite bloom" and the peak in crustal production around 2.7 Ga. However, one can speculate on whether these are related to the onset of global-scale plate tectonics and the shutdown of Archean diapirism.

Structural geology and gold metallogeny of the New Britannia mine area, Snow Lake, Manitoba

Beaumont-Smith, C.J.

Manitoba Geological Survey, 360-1395 Ellice Ave., Winnipeg, MB R3G 3P2

Gold mineralization in the Snow Lake area demonstrates a strong spatial association with the hangingwall of the McLeod Road thrust fault. This relationship suggests a strong deformational origin for the mineralization. The gold mineralization is hosted by a sequence of mafic and felsic volcanic and volcaniclastic rocks, with gold deposits generally located adjacent to lithological contacts. Structural analysis documents the penetrative isoclinal F_1 fold intercalation of volcanic rocks comprising the thrust fault hangingwall. Associated with F_1 folding is the local development of an S_1 layer-parallel foliation, which is generally restricted to area of stratigraphic contacts. These D_1 fabric elements are overprinted by S-asymmetrical shallowly inclined F_2 folds associated with D_2 thrust faulting. The emplacement of quartz vein-hosted gold mineralization and the associated potassium-carbonate alteration assemblage are also overprinted by F_2 folding. These relationships constrain the age of gold emplacement to pre- to syn-D_2. Even though textural relationships suggest that the later stages of D_2 are coincident with gold emplacement, although the gold mineralization is potentially older and is remobilized during D_2.

Criteria for evaluating channel flow in ancient orogens, and an example from the SE Canadian Cordillera in support of Couette (transport) rather than Poiseulle (channel) flow

Carr. S.D.[1] and Simony, P.S.[2]

[1]*Ottawa Carleton Geoscience Centre, Department of Earth Sciences, Carleton University, 1125 Colonel By Drive, Ottawa, ON, K1S 5B6* scarr@earthsci.carleton.ca,
[2]*Department of Geology and Geophysics, University of Calgary, 2500 University Drive NW, Calgary, AB, T2N 1N4* pssimony@ucalgary.ca

Discrimination between Couette (transport) vs Poiseuille (channel) flow modes requires characterization of: timing and nature of deformation and metamorphism throughout both the flow zone, or infrastructure, and the overlying suprastructure; timing and amount of dislocation on the upper and lower boundaries of the flow zone; the nature of the leading edge of the flow zone and, importantly, a 4D approach – an understanding of infrastructure migration through time and space. Evaluation of the significance of channel flow requires integration of results with regional geology (e.g. origin of rocks in the flow zone and whether there is geologic coherence or incoherence; 3D size of a potential channel; geologic and geometric evolution of the orogen through time including timing constraints and provenance of sediment deposition in flanking basins). The channels that have been proposed for the Canadian Cordillera in SE BC lie primarily within two adjacent thrust sheets. They are limited in thickness and in width along strike, have a possible extrusion "porthole" of width along strike of <150 km, contain coherent markers, and have retained links to their suprastructure. Thus channel flow can not be considered to be a tectonically effective process. The ~400 km wide thrust belt is constituted largely of four major thrust sheets that evolved and were emplaced "in sequence" in the Cretaceous and Paleocene during the westward underthrusting of the North American craton. In the external zone, each sheet is thin skinned and carried by a thrust system. In the internal zone, there is a westward increase in thickness and in the importance of ductile shear within each sheet toward the core zone. In the core, each sheet has an infrastructure of metamorphic and migmatitic rocks that includes interfolded cover and basement under a suprastructure of previously deformed and emplaced rocks. There is no doubt about the importance of flow and ductile shear in the infrastructure of each sheet. That flow, however, was dominantly "transport" (Couette) flow, which was transferred eastward into transport on the basal thrust of the eastern part of each sheet. This geometric – kinematic framework of great thrust sheets is based on the facts of stratigraphy, mapped geometry and geochronology. Channel flow models must be considered within this framework.

Residual porosity as an explanation for ductile-brittle behaviour during dome extrusion: experimental constraints

Kennedy, L., Russell, K. and Nelles, E.

Earth & Ocean Sciences, University of British Columbia, 6339 Stores Rd, Vancouver, BC V6T 1Z4, lkennedy@eos.ubc.ca

Decompression of rising magmas causes gas exsolution and a concomitant increase in magma porosity. Slow ascent commonly results in cooling and crystallization of the residual melt on the same time scale. Thus, slow ascending magmas commonly produce domes that are typically at or below their glass transition temperature (Tg), or have undergone degassing-induced crystallization. These magmas can be either highly porous or nonporous. For example, high residual porosity indicates that the system had low permeability and was quenched before the porosity could be removed. This quenching of primary porosity could be induced by cooling of the melt to below Tg, or by crystallization of the melt to produce a solid framework.

Here, we demonstrate experimentally the effects of porosity on the strength and failure behaviour of dacite dome rocks. Our triaxial rock deformation experiments were run at confining pressures (Pc) of 0, 25, 50, and 75MPa, at room temperature and strain rates of ~1 x $10^{-4}S^{-1}$. Our starting material has both low (6-8%) and high (17-24%) porosities, a uniform bulk composition (65 wt% SiO2) and is either highly crystalline or has a glassy matrix. The low porosity dacite experiments show a progressive increase in peak strength (100-700 MPa) with increasing Pc and all cores show brittle behavior, characterized by a rapid stress drop. Run products contain macroscopic fractures with deformation extremely localized around the shear fractures. Experimentally deformed dacites show extreme grain size reduction and the production of gouge.

We ran two sets of experiments on low porosity rocks: one for which the gear train was stopped just at failure and one for which, after failure and creation of the fracture surface, frictional sliding continued along the fracture. Grain size from the experimentally-generated gouge was measured using a grain size laser particle analyzer. The vast majority of ultra-fine grained particles (< 20 μm) are produced at fracture (ie large stress drops), and further sliding creates more gouge but does not create more fine grained material. We propose that the fine grained gouge developed at Mount Saint Helen's formed as a result of the microseismicity and that transport of the material to the surface did not appreciably reduce the grain size below ~ 20 μm.

In contrast, the high porosity dacites are 3-4 times weaker than low porosity dacite. The mechanism of deformation is dominated by distributed cataclastic flow rather than localized faulting. There is no stress drop, no discrete slip surface and no gouge production.

Our experiments suggest that domes with low residual porosity will extrude via brittle fault zones accompanied by microseismicity (e.g., Mt. St. Helens), and feature carapaces of cataclastic gouge (e.g., 'whalebacks') such as observed at Unzen, Montserrat (Watts et al. 2002) and Mount St. Helen's (Cashman et al. 2009; Pallister et

al. 2009). Conversely domes extruded at or below Tg and having high porosity will lack microseismicity, deform by distributed cataclastic flow rather than localize faulting, and may produce more stable structures.

A fractured gas reservoir in a composite foreland basin, Sichuan Province, China

Kraus, J.

Sunwing Zitong Energy Ltd., 101-6th Ave SW, Calgary, AB T2P 3P4
jkraus@sunwing.com

The Sichuan basin has a protracted, two-stage tectono-sedimentary history: early marine, extensional, and later terrestrial, compressive. It originated on the Neoproterozoic western passive margin of the South China block, which collided with both the North China block and Tibet during the Upper Triassic Indosinian orogeny, resulting in the closure of the Paleotethys. Until the India–Eurasia collision during the Eocene Himalayan orogeny, Tibet's eastern flank was extruding episodically along the Longmenshan (Dragon's gate mountains). The weight of the basinward, SE-propagating nappes led to flexural foredeep development and their erosional debris constitutes its flysch infill. The northeasterly-trending Longmenshan had been considered a conventional fold-thrust belt. However, its small width (20-50 km) and minor crustal shortening can hardly explain its large vertical uplift at the margin of the earth's highest relief. The uplift mechanism is therefore considered by some to be inflation by the ductile lower crust ('channel flow'). Draping of southern China around the Indian indenter may have caused rotation of the Sichuan basin. The *in-situ* stress field is E–W and the current deformation of the Longmenshan is accommodated by dextral transpression. The Zitong (gas) block in the Longmenshan foreland hosts the Upper Triassic clastic, fluvial-alluvial Xujiahe ('Xu') formation at depth, which constitutes both source and overpressured, tight reservoir for natural gas. Matrix permeability is poor and production relies on natural and induced fractures. Large, very gentle, slightly asymmetrical anticlines act as structural traps. The ones closer to the Longmenshan trend parallel to its front whereas the more distal ones trend approximately orthogonal to it. There are no clear overprinting relationships, but sediment onlaps reveal their quasi-simultaneous initiation in the Upper Triassic. This folding also affects the Cretacous surface rocks (and Triassic ones elsewhere) indicating a prolonged history. Most folds are dismembered along reverse faults which root in a Mid-Triassic detachment that extends at least into the basin centre.

Almost all of 30 vertical gas wells have failed because they relied on matrix permeability. Steep fractures must be penetrated at high angles to achieve economic flow. Advantage must be taken of rock volumes in which fractures of different generations and orientations form networks. The distribution of fractures is predicted according to paleo-stress fields through time and geophysical data. A directional exploration well will reveal whether this prediction was realistic.

LiDAR, GIS and down-plunge cross sections

Langenberg, C.W.

Long Mountain Research 11439-56 Avenue Edmonton, AB T6B 2X3

Canadians, such as George M. Dawson and John A. Allan, were great mappers of mountains. Nowadays, the use of airborne LiDAR (an acronym for Light Detection And Ranging) is becoming more common in geological mapping. LiDAR systems employ intense pulses of light, typically generated by lasers, and sensitive optical detectors to receive the reflected pulses. Airborne LiDAR systems consist of a laser machine mounted beneath an airplane or helicopter that follows a predefined path. The ground is then scanned by means of tens of thousands of pulses per second emitted from the laser. In order to obtain measurements for the horizontal coordinates (x, y) and elevation (z) of the objects scanned, the position of the aircraft is determined using accurate differential GPS measurements and the distance from the aircraft to the ground calculated. A combination of LiDAR and GIS techniques allows the geology to be viewed down-plunge and to be compared to cross sections obtained by more traditional methods using software such as LithoTect and GaiaBase.

The Alberta Geological Survey purchased LiDAR data for a 33 square km area covering Turtle Mountain. Trees and buildings were removed by filtering and the resulting bare earth DEM shows details of rock structures, which are concealed in regular aerial photos mainly due to vegetation cover. Draping existing geological map over this DEM allows refinement of these maps. The trace of the Turtle Mountain Thrust as displayed on a GSC geological map from 1993 and a 2007 AGS map can be more accurately placed. In addition, the trace of the axial plane location of stratigraphic contacts of the Turtle Mountain Anticline can be accurately placed on the DEM. Contacts needed adjustments of up to 150 m on the existing maps.

The University of Lausanne (and the Canton de Vaud) obtained LiDAR images of the Morcles Nappe from Swisstopo, the Swiss Geo-information Centre. The geology of the 'Diablerets' map-sheet (from swisstopo) was draped over the DEM and GIS technology allowed the area to be viewed down-plunge. These views can be compared with down-plunge cross sections of cylindrical domains. In the Haute Pointe area, the precise location of the lower contact of the Urgonian (Barremian) lithostratigraphic unit could be shown to be 100 m southeast from the location mapped in the 1980's. In other areas, contacts were mapped more than 100 m away from their true location. Faults could also be located more precisely.

The remarkable feature about LiDAR is its capability to remove non-ground objects. LiDAR presents a valuable tool to recognize features that would otherwise remain obscured by vegetation. It is anticipated that this technique combined with improved cross sectioning methods will revolutionize geological mapping.

Fold evolution and development of mylonites in the Grenville Front Tectonic Zone southeast of Sudbury, Ontario, Canada

Li, C. and Zhang, D.

University of Western Ontario, London, ON N6A 5B7
cli246@uwo.ca

Folds in a shear zone can be of various origins. They can be inherited from earlier deformations or formed during the shear zone deformation. In the later case, the folded surface can also have different origins. It is generally hard to differentiate them from each other. The Grenville Front Tectonic Zone (GFTZ) is the NW part of the Grenville Province, and its width ranges from several kilometers to tens of kilometers. Within the GFTZ, several Front-parallel mylonite zones are developed. Detailed field mapping and structural analysis of the fabrics in the GFTZ enable us to correlate the folds within a major mylonite zone south of Coniston to those outside mylonite zones. We found that most of the folds within the mylonite zone are developed by folding earlier foliations, and their evolution is closely related to the development of the mylonite zone.

We identified four generations of folds outside the mylonite zones. The F_1/ F_2 folds are isoclinal folds associated with amphibolite facies metamorphism, migmatization, and are responsible for the development of a transposition foliation (S_{T1}) everywhere within the GFTZ. The F_3 folds are km-scale to tens-of-km-scale regional folds, folding the transposition foliation. F_3 fold axial planes intersect the Grenville Front at a high angle. The F_4 folds have a chevron style in general and are characterized by SW-NE trending fold axial planes. They are buckling folds and may develop axial plane foliations. Across the GFTZ, from SE to NW, strain localization becomes more and more common, and the F_4 axial plane foliations eventually become mylonite foliations and hence mylonite zones in the Grenville Front. The stereographic projection of the fold axes in the mylonite zone south of Coniston has similar patterns to those of F_4 folds outside it. These fold axes orientation cannot be explained by Hansen's method. However, they can be correlated to F_4 folds outside the zone. They are interpreted as F_4 folds at higher strain stages.

Therefore the development of F_4 folds is closely related to the formation of Front-parallel mylonite zones in the Grenville Front. The development of the GFTZ probably started with buckling of the existing transposition foliation (S_{T1}) forming F_4 folds, as a result of NW-SE convergence. With increasing strain, strain localization becomes more significant along F_4 fold axial planes, which leads to tectonic transposition and the formation of mylonite zones in the Grenville Front.

Timescales of compaction in volcanic systems

Russell, J.K.[1], Quane, S.L.[2] and Andrews, G.[1]

[1]*Volcanology & Petrology Laboratory, Earth and Ocean Sciences, University of British Columbia, 6339 Stores Rd, Vancouver, BC V6T 1Z4*
[2]*Department of Geology, Colorado College, Colorado Springs, Colorado*

Ultimately, all natural magmas vesiculate near the Earth's surface to produce bubble-rich melts that commonly foam to the point of fragmentation producing pyroclastic deposits. Vesiculation processes increase porosity and create permeability thereby increasing the efficacy of fluid escape and suppressing explosivity. Conversely, processes that destroy porosity and permeability, including bubble collapse, compaction, and welding, inhibit the escape of fluids and can produce overpressures leading to explosive behavior. Compaction and welding processes are pervasive in volcanic deposits and pertinent to: i) formation of spatter-fed clastogenic lava flows, ii) sintering of fragmental material in volcanic conduits, and to iii) welding of pyroclastic flow and fall deposits. The rate at which porous pyroclastic deposits compact and sinter (i.e., welding; cf. Grunder and Russell, 2005) governs the efficacy with which porosity (and ultimately permeability) is lost (Sparks et al., 1999). Ultimately, rates of welding reflect the aggregate rheological properties of the deposit.

Here, we present an ensemble of experimental results used to investigate the rheology of hot, porous, pyroclastic materials during compaction. We have used a GEOCOMP Loadtrac II device modified to perform constant displacement rate or constant load deformation experiments on large (7 x 4.5 cm) unconfined cores of pumice, lava, or sintered ash. The experiments are at temperatures (T ~ 800-900°C), load stresses (< 150 MPa), and strain rates (10^{-6} to 10^{-2}) consistent with the emplacement of pyroclastic flows. The effects of fluid pressure have also been studied experimentally by using a steel cell and piston system that permits high-T deformation experiments at controlled P_{H2O} (Robert et al. 2008). During deformation, the cores of ash accommodate strain mainly by shortening and reduction of porosity. Porosity loss creates a strain dependent rheology expressed by a marked and continuous increase in effective viscosity. Our experiments simulate compaction of natural pyroclastic deposits and provide the data to parameterize a relationship between the effective viscosity of the hot, porous deposit of ash (η), the viscosity of the melt fragments (η_o) and porosity (ϕ) of the deposit (Quane et al. 2009):

$$\log \eta = \log \eta_o - \frac{\alpha \cdot \phi}{1 - \phi}.$$

The optimal value for the parameter α, based on the experimental data, is 0.78 ± 0.15. This relationship is used to model compaction and welding of processes in ignimbrites and in volcanic conduits as a function of load, temperature and porosity. Our results indicate that welding and compaction processes in pyroclastic deposits (e.g., ignimbrites, conduits, etc.) can occur on timescales of tens of minutes to hours. At these timescales, welding is fully decoupled from cooling of the deposits and may be coupled to

depositional processes. Within volcanic conduits, welding processes operate on fragmented magma rapidly enough to eliminate porosity in a matter of hours, thereby sealing off permeability and supporting cyclical vulcanian-style explosive eruptions.

Investigating the evolution of the Big Turn, Grenville Orogen of central Ontario: progress report

Schwerdtner, W.M.[1], Klemens, W.P.[2], Lu, S.J., Yang, J.F., and Landa, D.[3]

[1]*University of Toronto, Toronto ON M5S 3B1, fried.schwerdtner@utoronto.ca*
[2] *Highland Gold Mining Ltd, 7 Balchug Street, 119034 Moscow, Russia*
[3] *BHP Billiton Diamonds Inc., 1202 4920–52nd Street, Yellowknife, NT X1A 3T1*

At the northeastern shore of Georgian Bay (Lake Huron), undulatory lithotectonic boundaries (LTBs) such as the NE–SW Grenville Front, and the Allochthon Boundary Thrust (ABT), and the basal contact of the Parry Sound domain assume a southerly or southeasterly strike. Similarly, between the towns of Haliburton and Minden, the westerly trending trace of the Central Metasedimentary Belt boundary (CMBb) curves towards the south (see Ontario Geological Survey Map 2544). This results in a 90° crook that appears to postdate the development of SE-plunging, mesoscopic S-folds in the CMBb walls.

In three dimensions, the crooked CMBb and other LTBs have the geometry of gently folded surfaces with interlimb angles of >120°. Nonetheless, the map pattern of the LTBs attests to a large-scale curve in the Grenville Orogen (Ontario) which we call the Big Turn. Regional ductile deformation would have modified the shape of the Big Turn if it was created prior to the Ottawan (1090 –1020 Ma) orogenic event. Similarly, NW–SE trending, 10 km-scale, upright folds in LTB surfaces may have been initiated during Ottawan thrusting, but the final geometry of the folds is likely related also to the post-thrust development of the Big Turn. We therefore focus special attention on the NW-SE upright folds and their late-Grenvillian structural elements.

NW–SE structures such as the conjugate Moon River synform and the Wahwashkesh-Ahmic Lakes antiform refold the NNE-striking, synformal Parry Sound domain. To delineate the pattern of hinge-normal shear components and thereby discriminate between the buckling and bending mechanisms of large-scale folding, we mapped the M/S/Z style of mesoscopic buckle folds. Results of our ongoing study confirm that the Moon River synform is a conjugate buckle fold apparently initiated by NE–SW shortening of the Ottawan thrust stack. The Parry Sound synform, on the other hand, qualifies as a bending fold generated during gravity-driven subsidence of the dense Parry Sound allochthon into lighter granitoid rocks (Ahmic, Rosseau and Shawanaga domains). Swarms of 990 Ma granite-pegmatite dikes transect the folded main foliation in the Wahwashkesh-Ahmic antiform (east half) and in parts of the Parry Sound synform investigated by us in 2006-09. The strike lines of the dikes have a NE–SW preferred orientation, which attests to a late-Grenvillian increment of NW–SE extension in the Ahmic and Parry Sound domains. If thick granite-pegmatite dikes have the same preferred orientation and are equally numerous in most other parts of the Central Gneiss Belt (central Ontario), then 990 Ma wall-rock dilation modified the geometry, or contributed significantly to the formation, of the Big Turn.

Structural geology of the Kluane Metamorphic Assemblage, southwest Yukon Territory, Canada

Stanley, B.F.[1], Lin, S.[1] and van Staal. C.[2]

[1]*Department of Earth and Environmental Sciences, University of Waterloo, ON,* *bstanley@scimail.uwaterloo.ca* *and* *shoufa@sciborg.uwaterloo.ca*
[2]*Natural Resources Canada, BC,* *cvanstaal@nrcan.gc.ca*

The Kluane Metamorphic Assemblage (KMA) is a 160 km long northwest-southeast striking belt of variable deformed pelitic sediments in the southwest Yukon Territory. It is located within the Coast Belt, which marks the mid-Cretaceous 'welding' of the Insular Belt to the previously accreted Intermontane Belt of ancient North America (Gabrielese et al., 1991). Geochemical and neodymium isotope studies define the assemblage as a homogeneously mixed package of sediments with juvenile oceanic and mature continental affinity interpreted as a back arc basin setting (Mezger, 1996). No detrital zircon ages have been recorded. Five phases of deformation have been previously recorded. Precise dating of the deformation events using K-Ar remains ambiguous due to static recrystallization caused by the intruding granitic Ruby Range Batholith during the Early Tertiary (i.e., D_{n+4}). Consequently, peak metamorphism of the KMA is associated with this intrusion (i.e., K-Ar and ^{40}Ar-^{39}Ar ages range from 42.5 Ma to 61.7 Ma; Mezger, 1996). The main goal of this study is two fold: 1) to complete a detailed internal geometric construction of the KMA and its contact relationships and 2) to constrain the age of the KMA protolith.

Preliminary results show that the KMA has recorded two major deformation events. No regional marker horizon is observed in the KMA and therefore, geological mapping has dominantly relied on cleavage/fold vergence relationships. The earlier major phase of deformation, D_{n+2}, contains the main penetrative, axial planar schistosity characterized by micas (i.e., chlorite, muscovite, and biotite). Isoclinal folds on the scale of centimetre to metre amplitude define this folding event. Consequently, this folding event can, but not always, give the rock a differentiated layering texture. Mineral stretching lineations, L_{n+2}, are observed sub-parallel to the D_{n+2} fold axis. The latter deformation event, D_{n+3}, is distinguished by tight and slightly asymmetric folds on the scale of centimetre to tens of centimetres amplitude. Axial planar cleavage is also present and sub-parallel to S_{n+2}. Consequently, monoclinic shape symmetry is superimposed on S_{n+2}. Mineral lineations are also present on this foliation plane but only locally. Both of these generations of deformation cumulate to define a southwest directed hanging wall up sense of shear believed to be the result of underplating of the KMA with the overriding North American plate during Mesozoic(?) subduction (Mezger, 1996).

Future work will focus on the internal geometry of the KMA based on the cleavage/fold vergence relationships mentioned previously. The work will entail supplementary geological mapping of the KMA to locate fold closures, a composite microtectonic investigation of the S_{n+2}/S_{n+3} relationship, and multiple detailed cross-sections. U-Pb detrital zircon analysis will be undertaken to constrain the age of the protolith and geochemical analysis of interlayered ultramafic rocks (i.e., olivine

serpentinites) is also currently underway to understand their relationship with the KMA and adjacent rock units. Finally, results will be compiled and interpreted to give an increased understanding of the tectonic model of the KMA during emplacement to ancient North America during the Mesozoic(?) to Cenozoic.

Gabrielse, H., Monger, J.H.W., Wheeler, J.O., and Yorath, C.J., (1991): Part A. Morphological belts, tectonic assemblages, and terranes; in Chapter 2 of Geology of the Cordilleran Orogen in Canada, H. Gabrielse and C.J. Yorath (ed.); Geological Survey of Canada, Geology of Canada, no. 4, pp. 15-28.

Mezger, J.E., 1997. Tectonometamorphic evolution of the Kluane Metamorphic Assemblage, SW Yukon: evidence for Late Cretaceous eastward subduction of oceanic crust underneath North America. Ph.D. thesis, University of Alberta, Edmonton.

NOTES

NOTES

Canadian Tectonics Group

2009 Annual Meeting

Pine Falls, Manitoba

Field Trip Guide

Structural geology and tectonic evolution of the Archean Rice Lake greenstone belt at Bissett, Manitoba

Scott Anderson
Manitoba Geological Survey
Scott.Anderson@gov.mb.ca

Introduction

The Rice Lake area is located 150 km northeast of Winnipeg, Manitoba, in the central portion of the Archean Rice Lake greenstone belt of the western Superior Province. This area is an important gold-producing district in Manitoba and includes the Rice Lake gold mine on the north shore of Rice Lake at Bissett, which is developed on a vertically-extensive quartz-carbonate vein system hosted by gabbro. With past production and a total reported resource of 2.3 million ounces (George, 2006), this deposit is the largest lode-gold deposit identified to date in the Province.

In 2004, the Manitoba Geological Survey initiated a program of 1:20 000 scale bedrock mapping, structural analysis, lithogeochemistry, U-Pb geochronology and Sm-Nd isotopic analysis in the Rice Lake area, with the intent of resolving geological problems identified by previous workers and providing an improved geological context and predictive framework for ongoing mineral exploration. Bedrock mapping took place in 2004 and 2005 (Anderson, 2004, 2005) and the results of this work were released as a comprehensive Geoscientific Report in the fall of 2008 (Anderson, 2008).

This guide provides an overview of the regional setting, stratigraphy, geochemistry and structural geology of Neoarchean supracrustal rocks in the central portion of the Rice Lake belt, in light of new results from MGS mapping. Also included is a road log and descriptions of the sites to be visited on the 2009 CTG field trip (see Figure 3 for stop locations). These sites were selected to emphasize key localities for elucidating the structural history and tectonic evolution of the Rice Lake area; readers interested in other, or more detailed, aspects of the local geology are referred to the report by Anderson (2008). UTM co-ordinates (NAD83, Zone 15) for each of the planned field trip stops are included in the road log.

Regional context

The Rice Lake greenstone belt is one of several strands of Neoarchean and Mesoarchean supracrustal rocks that, along with the Red Lake and Birch-Uchi belts in Ontario, define the

western segment of the volcano-plutonic Uchi Subprovince (Card and Ciesielski, 1986) of the western Superior Province (Figure 1). The Uchi Subprovince is flanked to the north by the mainly plutonic Berens River Subprovince and to the south by metasedimentary rocks and derived gneiss, migmatite and granitoid plutonic rocks of the English River Subprovince (Card and Ciesielski, 1986). Thurston et al. (1991) included the Berens River Subprovince and the Mesoarchean portions of the Uchi Subprovince in the continental 'North Caribou Terrane' (NCT), which has come to be generally regarded as the protocratonic nucleus of the western Superior Province (e.g., Stott and Corfu, 1991; Williams et al., 1992; Skulski et al., 2000; Percival et al., 2002, 2006a; Whalen et al., 2003).

North Caribou terrane

In Manitoba, the south margin of the NCT includes three main components: 1) dominantly tonalitic, 3.01–2.99 Ga, igneous complexes; 2) nonconformably overlying, 2.98–2.92 Ga, platform-rift sequences, and; 3) voluminous Mesoarchean (2.94–2.90 Ga) and Neoarchean (2.75–2.72 Ga) continental-arc plutons, collectively referred to as the Wanipigow River plutonic complex (e.g., Bailes and Percival, 2000, 2005; Percival et al., 2002, 2006a, b; Bailes et al., 2003; Whalen et al., 2003; Sasseville et al., 2006). The platform-rift sequences are preserved along the east shore of Lake Winnipeg (the Lewis-Story assemblage), north of Rice Lake (the Little Beaver assemblage), and at Wallace Lake (the Wallace assemblage; Figure 2). In the Wallace and Lewis-Storey assemblages, continental-platform arenite and pebble conglomerate contain single age populations of ca. 2.99 Ga detrital zircons (Davis, 1994; Percival et al., 2006b) and are overlain by komatiite–tholeiite flow complexes, with minor intercalated iron formations, that are thought to record ca. 2.98–2.92 Ga plume-related magmatism associated with continental rifting of the NCT (Percival et al., 2002, 2006b). Possible equivalent rocks in the Red Lake and Birch-Uchi belts are found in the Balmer assemblage (2.99–2.96 Ga), which is likewise interpreted as rift-related (*see* Pervical et al., 2006a, and references therein). The Little Beaver assemblage consists of strongly transposed psammitic and semipelitic schists, with minor iron formations and gabbro sills (Anderson, 2008), that likewise contain a single age population of ca. 2.99 Ga detrital zircons (McNicoll and Percival, unpublished data, 2001), and perhaps represent a deeper-marine facies of the platform sequence.

In the Garner Lake area, the south margin of the NCT includes a thick succession of heterolithic epiclastic rocks and fragmental calcalkalic dacite that is intruded by a ca. 2.87 Ga (Davis, 1994) layered ultramafic–mafic intrusion and conformably overlain by dacitic volcaniclastic rocks, iron formation and a thick subaqueous flow complex that ranges in composition from komatiite to Mg-tholeiitic basalt to calcalkalic basalt. Hollings et al. (1999) attributed the komatiite flows to plume-related magmatism within a volcanic-arc formed on, or marginal to, the NCT. These rocks, which are referred to as the Garner assemblage (Figure 2), may be equivalent to portions of the Ball (2.94–2.91 Ga), Bruce Channel (2.89 Ga) and/or Trout Bay (2.85 Ga) assemblage of the Red Lake and Birch-Uchi belts (*see* Pervical et al., 2006a, and references therein).

In the western and central portions of the Rice Lake belt, the south boundary of the NCT is defined by the Wanipigow Shear Zone (WSZ; Figures 1, 2), an east-southeast-trending, subvertical, crustal-scale structure, marked by a pronounced topographic lineament and late, fault-bounded, fluvial-alluvial basins. A coincident zone of interleaved tectonite, mylonite and phyllonite ranges up to 1.5 km wide and, north of Rice Lake, contains evidence of an early episode of sinistral-reverse oblique-slip shear, followed by a protracted, dextral, transcurrent shear deformation (Anderson, 2008).

Uchi subprovince

The Uchi Subprovince in Manitoba consists of subaqueously-deposited volcanic and derived epiclastic rocks, synvolcanic gabbro sills and tonalite plutons, and unconformably overlying terrestrial and marine sedimentary rocks, which collectively define the Rice Lake belt (RLB) south of the WSZ. The exposed portion of the belt trends southeast for a distance of 145 km, from the eastern extent of Paleozoic cover at Lake Winnipeg to just east of the Manitoba-Ontario border, and ranges up to 15 km wide. Regional aeromagnetic patterns indicate that the belt extends at least 150 km to the west beneath Paleozoic cover. The eastern extent of the RLB in Ontario is known as the Bee Lake belt.

U-Pb zircon geochronological data indicate that major volcanism in the Manitoba segment of the Uchi subprovince spanned roughly 30 million years, between 2745 and 2715 Ma, whereas overlying sedimentary successions were deposited shortly after cessation of major volcanism, within a roughly 15 million year time interval between 2715 and 2700 Ma (*see* Krogh et al., 1974; Ermanovics and Wanless, 1983; Turek et al., 1989; Turek and Weber, 1991; Davis, 1994, 1996; Percival et al., 2006b; Sasseville et al., 2006; Anderson, 2008). Following the terminology of Poulsen et al. (1996), volcanic rocks south of the WSZ are subdivided into the Bidou and Gem assemblages, whereas the younger sedimentary successions are subdivided into the Edmunds and San Antonio assemblages (Figure 2). Each displays significant differences in constituent rock-types and inferred depositional settings; the volcanic assemblages are also differentiated by geochemical signatures and, in part, U-Pb ages. As outlined below, these Neoarchean assemblages are interpreted to record back-arc, arc and arc-rift magmatism and synorogenic sedimentation within a north-verging subduction-accretion complex that developed over a span of roughly 50 million years along the NCT margin (e.g., Stott and Corfu, 1991; Poulsen et al., 1996; Sanborn-Barrie et al., 2001; Percival et al., 2002, 2006a, b; Bailes et al., 2003; Bailes and Percival, 2005).

Bidou and Gem assemblages

The Bidou assemblage consists of 'MORB-like' tholeiitic basalt flows and gabbro sills, intercalated epiclastic rocks, and 'arc-like' calcalkalic felsic volcaniclastic rocks that are interpreted to represent a continental arc/back-arc complex (e.g., Poulsen et al., 1996; Bailes et al., 2003; Bailes and Percival, 2005; Percival et al., 2006b). U-Pb zircon ages from the volcanic rocks and overlying sedimentary successions constrain this volcanism to ca. 2745–2715 Ma (*see* Bailes et al., 2003; Percival et al., 2006b; Anderson, 2008). The thickest and most complete section of the Bidou assemblage defines a map-scale anticline in the core of the RLB east of the Ross River tonalite pluton (Figure 2). West of the Ross River pluton at Rice Lake, the Bidou assemblage consists of an upright, homoclinal succession that dips moderately north and is at least 7.0 km thick. The ca. 2724 Ma Ross River pluton (Anderson, 2008) intrudes the Bidou assemblage and is part of a voluminous tonalite-granodiorite-granite suite emplaced coeval with the 2730–2715 Ma volcanic assemblages. The available age constraints indicate a correlation to the 2.75–2.73 Ga Confederation assemblage in the Red Lake and Birch-Uchi belts (Sanborn-Barrie et al., 2001; Percival et al., 2006a, and references therein), which is interpreted as an extended, and locally rifted, continental arc.

The Gem assemblage consists of tholeiitic and calcalkalic volcanic and subvolcanic intrusive rocks, with thick intercalations of derived epiclastic rocks, that overlie the Bidou assemblage in apparent conformity at Gem Lake, in the southeast part of the belt (Figure 2). In contrast to the essentially bimodal (basalt-dacite) Bidou assemblage, volcanic rocks in the Gem assemblage range in composition from basalt to high-silica rhyolite. U-Pb zircon ages from volcanic and overlying sedimentary rocks at the type locality at Gem Lake constrain volcanism to ca. 2730–

2715 Ma (*see* Turek et al., 1989; Davis, 1994, 1996). Subaqueous basalt and basaltic andesite flows at Gem Lake range in chemical affinity from tholeiitic ('MORB-like') to calcalkalic ('arc-like') and are associated with transitional to calcalkalic rhyolite, suggesting deposition in localized arc-rift settings within an extended arc (Bailes and Percival, 2005; Percival et al., 2006b; Anderson, 2008). In Ontario, age-equivalent rocks are found in the Bee Lake belt, as well as farther east in the 2723–2713 Ma St. Joseph assemblage (Percival et al., 2006a, and references therein).

San Antonio and Edmunds assemblages

Neoarchean terrestrial and basinal marine sedimentary sequences unconformably overlie the Bidou and Gem assemblages in several locations. The fluvial-alluvial San Antonio assemblage is disposed in a series of fault-bounded basins along the NCT–Uchi interface (Figure 2) and consists of pebbly cross-bedded arenite and polymictic conglomerate, with minor greywacke. Weber (1971) interpreted these rocks as continental delta deposits and noted their similarity to classical synorogenic 'molasse' sequences. At Rice Lake, the basal contact is a pronounced angular unconformity and U-Pb ages of detrital zircons indicate a maximum depositional age of 2705 Ma (Percival et al., 2006b). Probable local equivalents are found in the Hole River (<2708 Ma) and Guano Island (<2728 Ma) sequences at Lake Winnipeg (Percival et al., 2006b) and the Siderock Lake assemblage (<2709 Ma) at Siderock Lake (Sasseville et al., 2006), all of which apparently post-date major arc magmatism, as suggested by the absence of cross-cutting intrusions.

The Edmunds assemblage consists of greywacke-mudstone turbidites, with minor conglomerate, laminated chert and iron formations, which were deposited in a regionally extensive submarine fan along the south flank of the Rice Lake belt (Figure 2). As described by Weber (1971), an abrupt facies change and coincident lenses of tonalite-boulder conglomerate in the upper part of the assemblage indicate a rapid change in sediment source and supply rate, perhaps in response to a sudden uplift event and the onset of collisional orogenesis. Detrital zircon U-Pb analyses by Davis (1996) indicate deposition of the basal facies after 2725 Ma, whereas the upper facies includes detrital zircons as young as 2705 Ma. Correlative rocks in the adjacent Bee Lake belt contain clasts of 2703 Ma tonalite and are intruded by a 2696 Ma granodiorite pluton (*see* Lemkow et al., 2006), thereby constraining sedimentation at this location to ca. 2700 Ma. Abundant Mesoarchean detrital zircons in both the Edmunds and San Antonio assemblages (Davis, 1996; Percival et al., 2006b) point to the uplifted NCT margin as a major source of detritus, and clearly distinguish them from superficially similar rocks in the underlying volcanic assemblages.

English River subprovince

The English River subprovince is an east-trending belt of medium to high-grade metasedimentary rocks and associated granitoid plutonic rocks that ranges up to 50 km wide and flanks the Uchi subprovince to the south over a strike length of more than 700 km. Referred to as the Manigotagan Gneissic Belt in Manitoba (McRitchie and Weber, 1971), this belt ranges from 15 to 40 km wide and is bounded to the north by the Manigotagan Shear Zone, a subvertical mylonite that is traced for more than 100 km along strike in Manitoba and is continuous with the Sydney Lake–Lake St. Joseph Fault in Ontario (Figure 1). The metasedimentary rocks consist mainly of turbiditic greywacke and mudstone that were deposited in a submarine fan(s) after cessation of major volcanism in adjacent terranes (Davis, 1998). Detrital zircon ages span a range from 3080 to 2704 Ma, indicating that the sediment was largely derived from the NCT and Uchi subprovince, and was at least locally deposited after 2704 Ma (Corfu et al., 1995; Davis, 1998); regional constraints require sedimentation mainly between 2715 and 2700 Ma. These rocks are thought to represent higher-grade equivalents to the Edmunds assemblage in the adjacent Uchi

subprovince. Various tectonic scenarios have been postulated for the English River turbidites, including fore-arc (Langford and Morin, 1976; Breaks, 1991), back-arc (Pan et al., 1998) and foreland (Davis, 1998) basins. Hoffman (1989) interpreted the English River subprovince as an accretionary prism (*see also* Card, 1990), which incorporated a precursor fore-arc basin on the flank of the Uchi volcanic arc.

The sedimentary succession was intruded by voluminous diorite-tonalite-granodiorite plutons at ca. 2698 Ma, prior to regional deformation and high-T–low-P metamorphism at ca. 2691 Ma (Corfu et al., 1995), likely related to terminal collision of the North Caribou and Winnipeg River terranes (Percival et al., 2006a, b). Metamorphic mineral assemblages indicate that peak metamorphism varied from middle greenschist facies in the north to localized granulite facies in the south (McRitchie and Weber, 1971; Breaks, 1991). Late-tectonic granite plutonism at ca. 2663 Ga (Turek et al., 1989) and ca. 2660 Ma titanite (Corfu et al., 1995) record the waning stages of thermotectonism at the present level of exposure.

Local geology and stratigraphy

Supracrustal rocks exposed in the Rice Lake area comprise the Mesoarchean Little Beaver assemblage and the Neoarchean Bidou and San Antonio assemblages (Figures 2, 3); only the Neoarchean rocks will be examined on this field trip. The Little Beaver assemblage consists of interlayered psammitic and semi-pelitic schist, with minor iron formations and gabbro sills, and is intruded to the north by the Mesoarchean Wanipigow River plutonic complex. To the south, these rocks are juxtaposed with Neoarchean supracrustal rocks of the Rice Lake belt across the Wanipigow Shear Zone (WSZ). The Bidou assemblage is intruded at the base by the synvolcanic Ross River plutonic suite and both are unconformably overlain by the San Antonio assemblage.

Metamorphic mineral assemblages throughout the map area south of the WSZ indicate low to middle greenschist facies regional metamorphism, with the exception of narrow zones along the margins of the larger plutons of the Ross River suite, which locally contain upper greenschist to lower amphibolite facies assemblages. In the interest of brevity, however, the prefix ‘meta’ is not utilized and the rocks are described in terms of known or inferred protolith.

Bidou assemblage

The Bidou assemblage at Rice Lake is subdivided for descriptive purposes into four distinct lithostratigraphic units that trend generally west, dip consistently north and are informally termed, from south to north, the Independence Lake (IL), Rainy Lake road (RLR), Townsite (TS) and Round Lake (RL) units. Contact relationships and younging criteria indicate that these units define a north-younging stratigraphic succession.

The constituent volcanic rocks range in composition from basalt, through basaltic andesite and andesite, to dacite and rhyolite, and are interpreted to record magmatism in an extensional, possibly back-arc portion of a continental-margin magmatic arc. As shown schematically in Figure 4, abrupt lateral and vertical facies transitions, evidence of deep erosional scouring, and the predominance of coarse epiclastic deposits point toward a very dynamic depositional setting. Most of these deposits are composed of detritus that was significantly reworked in a subaerial to shallow-marine setting prior to final deposition in deeper water. The dominance of coarsely porphyritic dacite detritus and the apparent absence of significant accumulations of primary felsic pyroclastic material or felsic flows indicate deposition in the medial–distal portion of a volcaniclastic apron on the flanks of a subaerially exposed volcanic complex that was likely dominated by porphyry effusions and cryptodomes.

The IL unit, at the base of the studied section (Figures 3, 4), consists of subaerially-transported heterolithic debris flows and a thick succession of aphyric to coarsely plagioclase-phyric andesite flows and volcaniclastic rocks that were likely deposited in a shallow subaqueous setting. The overlying RLR unit, in contrast, contains a medial section of thin-bedded greywacke-mudstone turbidites, chert and heterolithic debris flows, with minor pillowed basalt flows, that records subaqueous sedimentation and effusive mafic volcanism within a relatively deeper water, restricted basin that is interpreted to have formed in the hangingwall of a synvolcanic subsidence structure (i.e., a synvolcanic fault). Five lines of evidence indicate the existence of this structure:

- On-strike portions of the RLR and IL units exhibit significant differences in lithofacies and geochemical affinity.
- The interface between the on-strike portions of the RLR and IL units is invaded by synvolcanic intrusions and hypabyssal dike swarms, including a major apophysis of the Ross River pluton (Figure 3).
- The RLR-IL interface coincides with occurrences of stringer-style chlorite (Fe-Mg) alteration, laminated sulphidic chert, and solid sulphide layers in the RLR unit, which are indicative of fault-controlled hydrothermal circulation and seafloor discharge.
- The map pattern of an overlapping mafic flow complex indicates a significant change in unit thickness across the RLR-IL interface.
- Facing criteria indicate an angular discordance between the RLR unit and overlying rocks, which is interpreted to result from syn- to early-post–depositional tilting of the RLR unit in the hangingwall of the subsidence structure.

The upper portion of the RLR section consists of pillowed and massive flows and voluminous sills composed of MORB-like tholeiitic basalt. Pillowed flows predominate and define two major flow complexes separated by a gabbro laccolith that is interpreted to be rooted in the subsidence structure. The lower complex is approximately 450 m thick and conformably overlies stratified epiclastic rocks in the hangingwall of the structure, whereas the upper complex overlaps the structure and ranges from 50 to 200 m thick on the west to >600 m thick on the east, possibly as a result of synvolcanic growth-faulting.

U-Pb analyses of zircon from a felsic volcanic conglomerate layer near the top of the medial section of the RLR unit indicate a maximum age of 2727 ±2 Ma for the final increments of basin infilling and the associated extrusion of voluminous flows of MORB-like tholeiitic basalt (Anderson, 2008).

The Ross River plutonic suite intrudes the IL and RLR units, and may represent the subvolcanic equivalent of felsic epiclastic rocks at the base of the overlying TS unit. U-Pb analyses of igneous zircon from the pluton yielded a best-estimate emplacement age of 2724 ±1 Ma (Anderson, 2008), which represents the minimum age for the RLR unit. Emplacement of the Ross River pluton may have been, at least in part, controlled by the synvolcanic subsidence structure.

To the north, the upper contact of the RLR unit coincides with the trace of the Normandy Creek Shear Zone (NCSZ) and is unexposed. An angular discordance between the overlying TS unit and at least the lower portion of the RLR unit is indicated by facing criteria on either side of the NCSZ, where bedding in these units faces in opposite directions on the first regional cleavage, indicating that the discordance existed prior to the first regional deformation. Syn- to early-post–depositional tilting of the RLR unit in the hangingwall of a subsidence structure would readily explain this discordance, and is in keeping with the observed lithofacies and basin geometry. Although it is not possible to entirely rule out a fault contact, any such fault would have to be a

low-angle structure that predated deposition of the San Antonio assemblage, which stitches this contact to the west.

The TS unit consists of fluvial-alluvial volcanic sandstone and heterolithic volcanic conglomerate at the base, overlain to the north by pillowed flows of transitional arc-like basalt and a thick package of crystal-rich volcaniclastic rocks of dacitic composition. The epiclastic rocks are intruded by a thick gabbro sill that hosts the Rice Lake gold deposit and is interpreted as a subvolcanic equivalent to the pillowed basalt flows. A clastic dike at the base of the TS unit contains a unimodal population of ca. 2723 Ma detrital zircons (Anderson, 2008), which provide a maximum age for the unit as a whole. The western boundary of the TS unit is defined by the angular unconformity at the base of the San Antonio assemblage, which dips steeply northeast and is overturned in this location (i.e., the TS unit and San Antonio assemblage are arranged 'back-to-back'; Figure 3).

The RL unit defines the top of the Bidou assemblage at Rice Lake and consists of a basal heterolithic volcanic conglomerate unit, overlain to the north by a succession of felsic volcaniclastic and epiclastic rocks (Figures 3, 4). The basal conglomerate includes minor layers of sanukitoid-affinity basalt tuff, which are geochemically similar to hypabyssal diabase dikes in the underlying RLR and TS units. Felsic epiclastic rocks at the top of the RL unit contain hypabyssal quartz-feldspar porphyry intrusion that returned a U-Pb zircon age of 2715 ±2 Ma (Anderson, 2008), which provides a minimum age for the RL unit and appears to represent the waning stages of Neoarchean magmatism in the Rice Lake belt.

The GC unit (Figure 3) is a structurally bound and intensely transposed package of intermediate volcaniclastic, epiclastic and effusive rocks, basalt flows and gabbro, and minor dikes and sills of quartz-feldspar porphyry, that is tentatively correlated with the Bidou assemblage on the basis of comparable rock types and chemistry. The GC unit is structurally separated from the Rice Lake section of the Bidou assemblage by west-facing sedimentary rocks of the San Antonio assemblage, which are inferred to be younger on the basis of regional geological and geochronological constraints, and the conspicuous absence of crosscutting intrusions. Map patterns of these units define a macroscopic train of tight upright folds, which include the Horseshoe Lake anticline and Gold Creek syncline (Figure 3). Facing criteria in the in the hinge of the Horseshoe Lake anticline indicate that the GC unit also faces west and thus describes an older-over-younger relationship with the San Antonio assemblage. The contact between these units is therefore interpreted as a thrust fault, along which the GC unit was emplaced atop the San Antonio assemblage prior to regional folding.

San Antonio assemblage

The San Antonio assemblage consists mainly of planar and trough-cross bedded quartz arenite, with subordinate lenses of polymictic conglomerate, which are interpreted to represent channel-fill deposits in a braided fluvial system. Greywacke-mudstone turbidites in the northern portion of the assemblage likely represent a more distal, marine-fan facies of the system. These rocks define a 1.2 km thick succession that describes a broadly S-shaped map pattern that cuts across the regional strike of the Rice Lake belt (Figure 3). Bedding consistently faces west on the main regional cleavage, which is axial planar to the Horseshoe Lake anticline and Gold Creek syncline. The San Antonio assemblage overlies the Bidou assemblage along a pronounced angular unconformity that is exposed approximately 600 m northeast of Red Rice Lake (Stockwell, 1938; *see also* Poulsen et al., 1996; Figure 5).

In marked contrast to adjacent rocks of the Bidou assemblage, no intrusions are known to cut the San Antonio assemblage. Along the south margin of the greenstone belt west of Rice Lake,

the San Antonio assemblage nonconformably overlies tonalite of the Ross River plutonic suite. Here, a wedge-shaped unit of clast-supported and monolithic tonalite-boulder conglomerate at the base of the San Antonio assemblage records deposition by either debris-flow or rock-fall mechanisms at an abrupt topographic break.

In keeping with the results of previous detrital zircon studies of the fluvial-alluvial and basinal marine successions that unconformably overlie the Bidou assemblage (e.g., Davis, 1996; Percival et al., 2006a; Anderson, unpublished data, 2006), detrital zircons in a sample of greywacke from the San Antonio assemblage define two distinct age clusters at 2705–2747 Ma and 2938–3006 Ma (Anderson, 2008). The younger cluster has a weighted-average age of 2732 ±8 Ma, which is a conservative estimate for the maximum depositional age of the greywacke. The maximum depositional age of the San Antonio assemblage as a whole is further constrained by the 2715 ±2 Ma age obtained from the quartz-feldspar porphyry in the RL unit, which is truncated at the basal unconformity. Percival et al. (2006a) reported a 2705 ±5 Ma age for the youngest detrital zircon grain obtained from a sample of arkose near the base of the assemblage, north of Red Rice Lake, which is considered the best estimate of the maximum depositional age.

Lithogeochemistry and Sm-Nd isotope geochemistry

Volcanic and plutonic rock types in the Rice Lake area are essential bimodal and are thus divided for descriptive purposes into mafic ($SiO_2 \leq 56$ wt. %, Fe_2O_3+MgO ≥ 15 wt. %; anhydrous) and felsic ($SiO_2 \geq 62$ wt. %, Fe_2O_3+MgO < 10 wt. %; anhydrous) sample suites.

Mafic volcanic and plutonic rocks

The mafic volcanic and plutonic rocks are composed of subalkaline basalt and basaltic andesite that exhibit a somewhat continuous variation from tholeiitic to transitional to calcalkalic geochemical affinity. Three distinct geochemical subsuites are recognized (Figure 6):

‘MORB-like’ tholeiitic basalt

This basalt is found in the IL unit as diabase dikes; in the RLR unit as massive, pillowed and brecciated flows, and thick sills; and in the GC unit as a massive flow. The basalt is mostly Fe-tholeiitic and exhibits relatively flat profiles on extended-element plots normalized to normal mid-ocean-ridge basalt (NMORB) and primitive-mantle (PM; $La/Yb_N = 1.0–2.6$). These profiles show weakly fractionated light REE and heavy REE, and weak negative Nb anomalies (Figure 6a, b). In relation to NMORB, the light REE (LREE) are generally weakly enriched, whereas the heavy REE (HREE) are mostly depleted, and most samples exhibit evidence of weak Zr depletion. A sample of pillowed basalt in the RLR unit has an initial ε_{Nd} of 1.4 (at 2.73 Ga), suggesting minor interaction with isotopically evolved (i.e., older) crust.

The HFSE and REE abundances in the ‘MORB-like’ basalt indicate a chemical affinity to modern back-arc basin basalt, which is generally thought to result from partial melting of a depleted mantle source that interacted with a slab-derived aqueous fluid and/or melt component (e.g., Sinton and Fryer, 1987). Facies associations and stratigraphic relationships in the RLR unit indicate that this magmatism was associated with the development of a restricted marine basin in the hangingwall of a synvolcanic subsidence structure in the IL unit, and is therefore interpreted to record the initiation of a back-arc basin within the Bidou volcanic arc (Anderson, 2008).

‘Arc-like’ tholeiitic basalt

This basalt forms massive, pillowed and brecciated flows and related gabbro sills in the TS unit, and occurs as sills in the GC unit. Samples of this material exhibit weakly to moderately sloped profiles on NMORB- and PM-normalized extended-element plots ($La/Yb_N = 1.7–11.1$),

with moderately enriched and fractionated LREE, generally unfractionated HREE, prominent negative Nb anomalies and weak negative Zr and Ti anomalies (Figure 6c, d).

HFSE and REE abundances of this basalt are most similar to modern volcanic-arc basalt, which is thought to be derived via partial melting of the mantle wedge above a subducting slab of oceanic lithosphere, with contributions of slab-derived aqueous fluid and/or melt (e.g., Pearce and Peate, 1995). At Rice Lake, this 'arc-like' basalt is interpreted to indicate a resurgence of arc-magmatism subsequent to the initiation of back-arc spreading.

Sanukitoid-like transitional basalt

This basalt is found in the RLR and TS units as diabase dikes and in the RL unit as a thin fragmental unit, which is interpreted as a proximal scoria deposit. This basalt is of transitional tholeiitic–calcalkalic affinity, with 45–51 wt. % SiO_2, 0.8–1.0 wt. % TiO_2 and 9–11 wt. % Fe_2O_3 over an Mg# range of 61–70. NMORB- and PM-normalized extended-element plots exhibit steeply-sloped profiles with extreme La/Yb_N ratios of 20.2–55.8, given the high Mg# values. The profiles are characterized by strongly enriched and fractionated LREE, depleted and fractionated HREE and very pronounced negative Nb, Zr and Ti anomalies (Figure 6e, f). Chromium and nickel values are highly elevated and range from 231 to 408 ppm (average 322 ppm) and from 101 to 402 ppm (average 233 ppm), respectively. A sample of the scoria layer in the RL unit has an initial ε_{Nd} value of 1.2 (at 2.715 Ga) and a crustal-residence model age (T_{CR}) of 2.91 Ga, suggesting derivation from melts that interacted with older, isotopically evolved crust.

The unique chemistry of this basalt (high Mg#, Cr and Ni, with strongly enriched LREE and LILE) indicates an affinity to the Late Archean sanukitoid suite. As described by Shirey and Hanson (1984), the petrogenesis of these rocks is generally thought to involve partial melting of sub-arc mantle peridotite that was extensively metasomatized by slab-derived fluids (*see also* Stern, 1989; Stern et al., 1989). At Rice Lake, this basalt is interpreted to signal a change toward more evolved magmatism in the advanced stages of the Bidou volcanic arc.

Felsic volcanic and plutonic rocks

Felsic volcanic and plutonic rocks of the Bidou assemblage at Rice Lake exhibit bulk dacitic compositions and calcalkalic geochemical affinities. Although most are subalkaline, some samples also appear to exhibit elevated Nb in relation to Y, suggesting a mildly alkaline affinity. Chondrite-normalized extended-element profiles (Figure 7a) are smoothly-sloped, with enriched and fractionated LREE (La/Yb_N = 9.4–57.8; La/Sm_N = 3.3–6.3) and weakly to moderately fractionated HREE (Gd/Yb_N = 1.7–6.9); negative Eu anomalies are lacking (Eu/Eu* = 0.9–1.5). All samples exhibit strong negative Nb anomalies on primitive mantle–normalized profiles (Figure 7b), with generally weak positive Zr and weak negative Ti. A sample of brecciated dacite in the RLR unit has an initial ε_{Nd} of 0.3 (at 2.73 Ga) and a crustal-residence model age (T_{CR}) of 3.03 Ga, whereas a sample of quartz-feldspar porphyry (QFP) rhyolite in the RL unit has an initial ε_{Nd} of 1.1 (at 2.715 Ga) and a crustal-residence model age (T_{CR}) of 2.94 Ga, both of which are consistent with derivation from melts that interacted with older, isotopically evolved crust.

The HFSE and REE concentrations of the felsic volcanic and plutonic rocks indicate a chemical affinity to the 'FI' felsic volcanic rocks described by Lesher et al. (1986), which are generally interpreted to be derived from low-degree partial melting of metasomatized mantle-wedge peridotite, with variable contamination by crustal material, in suprasubduction-zone settings (Barrie et al., 1993). A subset of the these samples is characterized by relatively high Mg# values, high contents of Cr, Ni and Sr, anomalously low contents of Y and Yb, strongly fractionated REE patterns and correspondingly high Sr/Y and $(La/Yb)_N$ ratios. These attributes indicate a chemical affinity to Cenozoic adakite, which is a distinctive suite of high-silica igneous

rocks in oceanic and continental-arc settings that is considered to be the direct product of partial melting of subducting slabs of young, hot oceanic lithosphere (e.g., Defant and Drummond, 1990; Martin et al., 2005). More recently, however, others have suggested that adakite-like compositions can be produced from mantle-wedge–derived magmas by simple fractionation and contamination processes in the upper plate, without direct contributions from slab melts (e.g., Richards and Kerrich, 2007). Regardless of petrogenetic model, the presence of adakite-like rocks at Rice Lake strongly implies a supra-subduction–zone setting. Initial ε_{Nd} values and crustal-residence model ages (T_{CR}) indicate derivation from melts that interacted with older, isotopically evolved crust, suggesting that the Bidou arc formed on, or close to, the margin of the NCT.

Structural geology

Ductile and ductile-brittle deformation structures in the Rice Lake area are subdivided into six generations (G_1–G_6; Table 1) on the basis of overprinting relationships. In areas of poor exposure, the style of deformation structures and their patterns of orientation were also used for correlation. The observed structures include planar fabrics (e.g., foliations, cleavages, shear bands, flattened clasts), linear fabrics (e.g., mineral, stretching, slickenline and intersection lineations) and/or folds, which are denoted in the text and figures by S_x, L_x and F_x, respectively, where 'X' indicates the assigned generation. Intersection lineations are denoted by L^X_Y, where 'X' and 'Y' refer to the generations of intersecting planar fabrics. In any given outcrop, the mesoscopic deformation structure is usually dominated by three distinct generations of planar fabric, which are assigned to the G_3, G_4 and G_5 generations (hence, S_3, S_4 and S_5). These fabrics are present in the San Antonio assemblage, which indicates that penetrative regional deformation occurred after ca. 2705 Ma, the maximum depositional age of these rocks as documented by Percival et al. (2006a).

G_1 structure

Meso- and microscopic examples of G_1 deformation structure are identified in very angular to subrounded fragments of sericitic and quartzofeldspathic phyllite in a heterolithic clastic dike near the base of the TS unit. The G_1 structure consists of a continuous to finely spaced S_1 foliation defined by very fine grained sericite and chlorite. In some fragments, quartz (±feldspar) exhibits undulose extinction, lattice-preferred orientation, serrated grain margins and a weak shape-preferred orientation, which are indicative of dynamic recrystallization under greenschist-facies metamorphic conditions. The S_1 fabrics show misalignment between fragments, do not extend across the boundaries of individual fragments and are not observed in the generally massive chloritic sandstone matrix of the clastic dike, thereby indicating that they predate fragment entrainment. The unimodal (ca. 2723 Ga) zircon population in the clastic dike and the delicate shapes of the phyllite fragments suggest a very proximal source of exhumed volcanic-arc rocks, which were either subaerially exposed during the initial depositional stages of the TS unit or were in a near-surface setting (and were sampled) by the clastic dike during emplacement. For these reasons, the S_1 fabrics are interpreted to be broadly synvolcanic and a result of deformational processes within the Bidou volcanic arc. The synvolcanic subsidence structure east of Rice Lake likely represents a macroscopic G_1 structure.

As described by Bruhn et al. (1994), phyllic (i.e., sericitic) mineral assemblages and phyllite are observed in the deeper parts of normal faults, where they form as a consequence of high heat flow and hydrothermal circulation during active displacement. In such systems, continued displacement on the controlling faults, coupled with active erosional denudation, may result in rapid exhumation of phyllic footwall rocks. A similar mechanism is envisaged for the Rice Lake area, where exhumed rocks in the immediate footwalls of synvolcanic subsidence structures are considered a likely source of phyllite fragments.

G_2 structure

Structural facing criteria in the GC unit of the Bidou assemblage and the younger San Antonio assemblage indicate that both face west on the west-northwest-trending axial-planar S_3 fabric associated with the F_3 Horseshoe Lake anticline (*see* below), and thus describe an older-over-younger structural relationship that must predate regional F_3 folding (Figure 3). For this reason, the upper contact of the San Antonio assemblage is interpreted as a thrust fault, which is assigned to the G_2 generation of deformation structure on the basis of the macroscopic field relationships described above. Due to a combination of poor exposure and a generally intense structural overprint, mesoscale structural or kinematic evidence in support of this hypothesis is generally lacking. In most locations, the contact coincides with a zone of sericitic tectonite that appears to record multiple generations of fabric development, yet fails to provide convincing evidence of a deformation fabric that might correspond to the G_2 generation. Nevertheless, several examples of a G_2 deformation fabric are preserved in bedded arenite of the San Antonio assemblage, in locations immediately below the inferred position of the macroscopic G_2 thrust fault, as well as deeper down-section. This fabric comprises a penetrative and continuous shape fabric (S_2) defined by fine-grained foliated sericite and elongate quartz grains that roughly parallels bedding and is folded around the hinges of mesoscopic, open to tight folds that are interpreted to be parasitic to the macroscopic F_3 closures.

G_3 structures

The earliest regionally pervasive deformation structure observed in the Rice Lake area is a planar-linear (S-L) shape fabric that is most prominently defined on a mesoscopic scale by flattened and stretched primary features (e.g., feldspar phenocrysts, clasts, amygdules, pillows, etc.). On a meso- to microscopic scale, the shape fabric typically includes a continuous foliation defined by fine-grained chlorite, actinolite and sericite. The planar fabrics, which are assigned to the G_3 generation of deformation structures, generally trend west-northwest and dip steeply to moderately north. The associated L_3 stretching lineation plunges moderately to the northeast in the plane of the S_3 fabric. The axial ratios of stretched and flattened primary features are highly variable but typically in the range 2–5:1 (Y:Z, X:Z and X:Y); finite strain determinations performed by Lau and Brisbin (1996) on porphyritic samples indicate strain ellipsoids that vary from constrictional to flattening type. The G_3 shape fabric is generally symmetric (e.g., Lau and Brisbin, 1996) except where overprinted by later deformation, and is thus interpreted to indicate the predominance of pure shear over simple shear. From north to south across the Rice Lake area, the L_3 lineation exhibits a systematic change in trend and plunge, from steeply or moderately north-northeast plunging in the south to shallowly east plunging in the north (Figure 8). This change is interpreted to result from later reorientation during dextral transcurrent shear on the WSZ (e.g., Poulsen et al., 1986).

In the TS and RL units, the S_3 fabric is consistently oriented at a shallow counter-clockwise angle to bedding (which thus faces east on S_3), and mesoscopic examples of F_3 folds are very rare. Across the Normandy Creek Shear Zone in the RLR unit, S_3 is consistently oriented clockwise to bedding (which thus faces west on S_3), and is axial planar to open to tight, S-asymmetric folds that plunge shallowly northwest. In both of these areas, S_3 dips more steeply than bedding. Widely separated examples of bedding in the IL unit show both clockwise and counter-clockwise relationships to the S_3 fabric. West of Rice Lake, the S_3 fabric passes continuously into the San Antonio assemblage, where it is most prominently defined by a preferred alignment of elongate pebbles in conglomerate and channel-lag deposits; the L_3 fabric is generally not well developed in these rocks. In most outcrops, the S_3 clast elongation is significantly oblique to bedding and thus constrains the macroscopic F_3 fold geometry.

In the San Antonio assemblage and GC unit, the S_3 fabric exhibits an axial planar relationship to the Horseshoe Lake anticline (HLA) and Gold Creek syncline (GCS), which are the most prominent closures in a macroscopic train of folds that trends across the regional structural grain of the belt (Figure 3). These folds are tight, steeply inclined and asymmetric structures that are assigned to the third generation (G_3) of deformation structures on the basis of overprinting and bedding-cleavage (S_0-S_3) relationships. In the San Antonio assemblage, bed forms and indicate that the F_3 folds are overturned to the southwest, with upright limbs that dip moderately to steeply northeast and overturned limbs that dip steeply in the same direction. On the shared limb of the HLA and GCS, south of Horseshoe Lake, the S_3 fabric is refracted toward the west-southwest in quartz arenites of the San Antonio assemblage, presumably in response to a higher competence as compared to the adjacent volcanic and volcaniclastic rocks. Map patterns and the absence of S_0-S_3 vergence changes in the TS and RL units of the Bidou assemblage indicate that the macroscopic F_3 fold train terminates at the base of the San Antonio assemblage. As described by Bailes (1998), this relationship is best explained in the context of the pronounced angular unconformity in this location, which must have been configured such that the maximum principal stress during folding was oriented subparallel to the primary anisotropy (i.e., bedding) in the San Antonio assemblage but suborthogonal to that in the underlying units. Hence, the younger rocks accommodated the regional shortening by buckling and folding, with some flattening, whereas the older rocks experienced layer-subparallel flattening without buckling.

In general, minor fold hinges and bedding-cleavage (S_0-S_3) intersection lineations associated with the GCS plunge shallowly northwest or southeast, whereas those in the HLA plunge more steeply. In the footwall of the San Antonio assemblage, this change in F_3 plunge is mimicked by the systematic change, from south to north, in the trend and plunge of the L_3 lineation, which maintains a near-orthogonal angular relationship with the macroscopic hinge in the adjacent segment of the F_3 fold train. From these relationships, the G_3 linear structures are interpreted to have developed contemporaneously within a regional kinematic frame of northeast-southwest shortening. Towards the north, these structures appear to have been reoriented, in a sympathetic manner, in response to dextral transcurrent shear along the south margin of the WSZ, as suggested by Poulsen et al. (1986).

On the north margin of the WSZ, psammitic and semipelitic rocks of the Little Beaver assemblage exhibit a penetrative and pervasive foliation defined by a preferred alignment of micaceous minerals, quartz segregations and elongate garnet porphyroblasts. In these rocks, the foliation parallels a locally well-developed gneissosity defined by alternating quartzofeldspathic and micaceous domains. In some outcrops, a weak to moderate stretching and mineral lineation is also developed, and plunges moderately to the northeast in the foliation plane. The foliation is axial planar to tight to isoclinal folds of quartz segregations and the gneissosity. Some of these folds are rootless and markedly noncylindrical. Kinematic indicators in the quartzofeldspathic layers, which include asymmetric boudins, shear-bands and S-C fabrics, consistently indicate sinistral-reverse oblique-slip shear. In contrast, the same types of kinematic indicators in the more micaceous semipelite layers consistently indicate dextral strike-slip shear. From this relationship, it is inferred that the quartzofeldspathic (and presumably more competent) layers preserve an earlier generation of deformation structures associated with a sinistral kinematic frame, whereas the semipelitic (and presumably less competent) layers preserve evidence of younger shear deformation within a dextral kinematic frame. Based on their orientation and kinematics, which are consistent with northeast-southwest shortening, the earlier structures are correlated with the G_3 structures south of the WSZ in the Rice Lake belt.

The overall geometry of G_3 structure in the Rice Lake area supports a model of regional sinistral transpression in which strongly partitioned northeast-southwest shortening is manifested

by three different styles of deformation in three distinct structural domains: 1) sinistral-oblique noncoaxial shearing within a precursor to the WSZ, 2) upright subhorizontal folding in those rocks structurally above the basal unconformity of the San Antonio assemblage, and 3) bulk flattening and subvertical stretching in those rocks below.

G_4 structures

Throughout the mapped area, the S_3 shape fabric is overprinted at a shallow counter-clockwise angle by a variably developed crenulation cleavage attributed to G_4 deformation. The S_4 cleavage trends west or southwest, dips steeply north and is often best preserved as a finely spaced crenulation cleavage within flattened clasts that define the regional G_3 fabric. In these instances, the S_4 cleavage typically strikes 20–40° counter-clockwise to the intermediate (Y) axes of the flattened clasts. In many cases, this internal S_4 cleavage is sharply truncated at the margins of individual clasts, suggesting reactivation of S_3 during, or subsequent to, development of S_4. The S_4 cleavage transects meso- and macroscopic F_3 folds in the San Antonio assemblage, and intersects S_3 to form a prominent L^3_4 intersection lineation that generally plunges at moderate angles to the northeast. The L^3_4 lineation varies from parallel to slightly oblique to the L_3 stretching lineation, and likewise exhibits a shallower plunge along the south margin of the WSZ. The S_4 fabric is axial planar to rare, open to tight, Z-asymmetric folds that plunge moderately north. No examples of regional-scale F_4 folds are delineated in the Rice Lake area, and the G_4 structures appear to have accommodated weak northwest-southeast shortening of the Rice Lake belt, perhaps during the early increments of regional dextral transpression (*see* below).

G_5 structures

Fifth-generation ductile deformation structures are pervasive in the Rice Lake area, but are only penetrative in discrete high-strain zones, the most notable example of which is the regional-scale WSZ. This shear zone ranges up to more than 1.5 km thick and defines the interface between the NCT and the Uchi Subprovince, along the northern boundary of the mapped area. Other prominent examples of G_5 high-strain zones, which are generally about 50–100 m thick, include the Gold Creek, Normandy Creek and Red Rice Lake shear zones (Figure 3). South of Rice Lake, subsidiary G_5 high-strain zones splay towards the south off the Gold Creek and Red Rice Lake shear zones, the most prominent example of which is the Pilot–Smuggler Shear Zone described by Bailes (1971).

The G_5 high-strain zones are characterized by penetrative mylonitic foliations (S_5) that are defined by domains of fine-grained, foliated sericite and chlorite that alternate with domains of dynamically recrystallized quartz and feldspar. In coarsely porphyritic rock types, these mylonite zones preserve textural evidence of contemporaneous brittle failure of plagioclase and ductile flow of quartz, suggesting deformation at or near the brittle-ductile transition. The mylonitic foliation parallels an intense shape fabric defined by highly deformed primary features, including pillows and clasts. In many locations, these features delineate significant variations in apparent finite strain along and across strike in the G_5 high-strain zones. Although it is not possible to quantify the proportion of the accumulated strain that can be attributed to G_5 structure, the highest finite strains are recorded in coarse clastic rocks near the confluence of the Normandy Creek Shear Zone and the WSZ. In general, the S_5 fabrics and their host high-strain zones trend west-northwest to north-northwest and dip subvertically.

The G_5 high-strain zones typically contain a well-developed lineation defined by quartz-filled pressure fringes on porphyroclasts or pyrite cubes, stretched clasts, locally well-developed quartz ribbons and ridge-in-groove striations. The mylonitic foliation commonly envelops packets of strongly Z-asymmetric, open to tight, upright, chevron-style F_5 folds that exhibit highly variable plunges, from shallowly east to steeply north. Dextral kinematic indicators are well developed on

horizontal outcrop surfaces, and typically include S-C fabrics, σ-porphyroclast systems, shear bands and asymmetric boudins. Conjugate shear bands and shear fractures are a common feature of particularly high strain zones in the WSZ, as well as the NCSZ, suggesting a significant component of zone-normal shortening. The structural geometry of the G_5 structures indicates that they accommodated dextral transcurrent shear deformation in response to north-northwest–south-southeast shortening of the Rice Lake belt. This deformation was strongly partitioned into the discrete high-strain zones, which appear to be controlled by a combination of primary anisotropy and/or pre-existing structures.

South of the WSZ and outside the G_5 high-strain zones, the S_5 fabric is manifested as a regionally pervasive, spaced, fracture or shear-band cleavage that trends northwest or north-northwest and dips subvertically. The S_3 and S_4 fabrics are transposed in a dextral sense along the margins of the S_5 cleavage planes. On the scale of individual outcrops, this fabric is locally observed to intensify into discrete high-strain zones that, like the examples described above, are characterized by shallow-plunging lineations and well-developed dextral kinematic indicators on horizontal outcrop surfaces.

G_6 structures

The latest generation of ductile deformation, G_6, appears to be associated with an open, north-trending flexure in the Rice Lake area that is best defined by macroscopic map patterns in the TS unit. On a mesoscopic scale, outcrops in the hinge of this fold contain a weak to moderate, typically closely spaced, crenulation cleavage (S_6) that is associated with open, upright, steeply north-plunging, symmetric folds of the earlier generations of planar fabric. The S_6 cleavage generally dips steeply to the east-southeast. The G_6 structures are best developed along the south shoreline of Rice Lake. On the east limb of the macroscopic fold, the early fabrics (S_3, S_4, S_5) maintain their consistent overprinting relationships but have been rotated approximately 50° in a counter-clockwise sense into a more northeasterly trend. The G_6 structures appear to have accommodated east-west shortening of the Rice Lake area, perhaps in response to a buttressing effect along the northwest margin of the Ross River pluton during the late increments of north-northwest–south-southeast shortening of the belt.

Structural evolution

The orientation and style of the deformation structures, coupled with inferences drawn from associated kinematic indicators and macroscopic map patterns, indicate that the deformation history of the Rice Lake area likely involved five distinct episodes of regional deformation (D_1–D_5; Table 1; Figure 9), two of which (D_1 and D_2) predate deposition of the San Antonio assemblage and are interpreted to be broadly synvolcanic. In this scheme, each deformation episode is interpreted to represent a distinct kinematic frame. The distinction between deformation episode (D_X) and generation of deformation structure (G_Y) is used to emphasize the fact that more than one generation of fabric may form during a single episode of progressive deformation (e.g., Tobisch and Paterson, 1988). In the present case, the G_4–G_6 structures are interpreted to record progressive deformation associated with regional northwest-southeast (present co-ordinates) shortening, and are thus assigned to a single, possibly protracted, episode of deformation (D_5).

The predepositional G_1 fabric observed in fragments in the clastic dike at the base of the TS unit is attributed to high heat flow and hydrothermal alteration associated with synvolcanic normal faulting within the Bidou volcanic arc. This faulting likely coincided with the onset of mafic magmatism in the RLR unit, which exhibits a chemical affinity to back-arc basin basalt. In this regard, the G_1 fabric is interpreted to record an episode of arc extension and normal faulting

(D_1), possibly associated with the initiation of back-arc spreading along the inboard portion of the Bidou arc. Continued D_1 normal faulting of the RLR and IL units, prior to deposition of the TS unit, is interpreted to account for the angular discordance at the base of the TS unit.

In the Horseshoe Lake area, the map patterns of the San Antonio and Bidou assemblages indicate the existence, and provide evidence of the nature, of two temporally distinct deformation episodes (D_2 and D_3). The D_2 episode is not associated with any observed meso- or microscale deformation structures, but is indicated by the pronounced angular unconformity at the base of the San Antonio assemblage. In particular, the near-orthogonal orientation of the unconformity with respect to primary stratification in the rocks beneath indicates that the Bidou assemblage must have been tilted into a near-vertical orientation prior to deposition of the San Antonio assemblage (Figure 9; D_2). This tilting is ascribed to the D_2 deformation episode and is inferred to result from accretionary processes along the southern margin of the NCT, perhaps in association with tectonic inversion of the Bidou back-arc.

West of Horseshoe Lake, the older-over-younger map pattern of the Bidou and San Antonio assemblages is interpreted to indicate the presence of a G_2 thrust fault, formed during the D_3 deformation episode (Figure 9; D_3). Although the kinematics of the D_3 episode remain unknown, it is interpreted to have accompanied tectonic inversion of the San Antonio basin, perhaps as a consequence of accretionary processes along the NCT margin or in the initial stages of crustal thickening associated with terminal collision of the NCT and Winnipeg River terrane (i.e., the Kenoran Orogeny).

The D_4 deformation episode, as recorded by G_3 deformation structures, was strongly partitioned into macroscopic domains of sinistral-oblique noncoaxial shearing (WSZ), bulk flattening and subvertical stretching (Bidou assemblage at Rice Lake), and upright subhorizontal folding (San Antonio assemblage and the GC unit of the Bidou assemblage, west of Rice Lake; Figure 9; D_4). The geometry and kinematics of the G_3 structures indicate a regional regime of sinistral transpression in response to north-northeast–south-southwest shortening (present co-ordinates) of the Rice Lake belt. This deformation likely coincided with major crustal thickening during the main collisional stage of the Kenoran Orogeny.

The G_4, G_5 and G_6 structures are interpreted to record progressive deformation (D_5) within a regional regime of late-orogenic dextral transpression associated with the terminal phase of the Kenoran Orogeny. The G_4 structures consist of a penetrative to finely spaced crenulation cleavage that transects the macroscopic F_3 folds west of Rice Lake and appears to have accommodated weak northwest–southeast shortening (present co-ordinates) during an early increment of D_5 transpression (Figure 9; early D_5). The G_5 structures include a series of generally west-northwest-trending, ductile>brittle, high-strain zones, as well as a regionally pervasive fracture or shear-band cleavage that trends northwest. The high-strain zones contain mylonitic foliations, shallowly plunging lineations, packets of strongly Z-asymmetric folds and well-developed dextral kinematic indicators on horizontal outcrop surfaces, and are interpreted to have accommodated strongly partitioned north-northwest–south-southeast shortening during main-stage D_5 transpression (Figure 9; main D_5). The G_6 structures are associated with an open, north-trending flexure of the Bidou assemblage in the Rice Lake area that may be related to a local strain perturbation in the hangingwall of the Normandy Creek Shear Zone, perhaps in response to a buttressing effect along the northwestern margin of the Ross River pluton during late-stage D_5 transpression (Figure 9; late D_5).

Field trip road log

Safety issues
Field trip participants are reminded that any geological fieldwork, including field trips, can present significant safety hazards. Foreseeable hazards on this field trip include inclement weather, slips and falls on uneven terrain, insect bites and stings, animal encounters, exposure to Poison Ivy, and flying rock from hammering. **The provision and use of appropriate personal protective equipment (e.g., rain gear, sunscreen, insect repellant, safety glasses, sturdy boots) is the responsibility of each participant.** To ensure the safety of bystanders, participants are asked to refrain from hammering rock. If deemed necessary, sample collection can take place after the group has departed each outcrop. Participants are asked to remain with the group at all times. A first aid kit and satellite telephone (for emergency purposes only) will be carried by the field trip leader.

From the parking lot of the Manitou Lodge in Pine Falls, turn right (east) onto Hwy 11 and travel 3.0 km to the intersection with Provincial Road 304. Turn left (north) onto PR304, cross the Winnipeg River at the Pine Falls hydroelectric generating station, and follow PR304 to the town of Bissett (119 km total driving distance). Note that PR304 is gravel-surfaced for the final 45 km of the drive, from just north of the bridge over the Manigotagan River to the town of Bissett.

Set odometer to zero upon arrival at the Post Office in Bissett (look for the dilapidated log cabin on the north side of PR 304, approximately 400 m east of Wynne's Place restaurant and store).

From Bissett drive 7.7 km east on PR304 to the junction with the Rainy Lake logging road on the right (look for the orange gate and millstones approximately 200 m south of PR304).

Park on south side of PR304 at the entrance to the logging road. Walk south on the logging road for 1.2 km (approx. 15 minutes travel time) to a low, south-facing outcrop ledge just off the left (east) shoulder of the road.

Stop 1 (319840mE, 5655241mN; NAD83, Zone 15):
Bidou assemblage, Rainy Lake Road unit

This outcrop exposes thin-bedded feldspathic greywacke, mudstone and chert in the medial section of the Rainy Lake Road unit of the Bidou assemblage (Figure 3). These rocks record subaqueous deposition via downslope turbidity flows into a relatively quiescent, deep-marine basin that is interpreted to have formed in the hangingwall of a synvolcanic subsidence structure (G_1) to the west. Planar beds dip at moderate angles to the northwest and include normal-graded beds with well-developed load casts that indicate these rocks are upright. Contorted and disrupted bed forms and asymmetric folds that lack an axial-planar cleavage are interpreted to represent soft-sediment slump structures; these are locally truncated by overlying beds. Open to tight S-folds of bedding with an associated fine-scale axial planar cleavage are interpreted to be parasitic to the macroscopic anticline (G_3) that dominates the structure in the eastern Rice Lake belt. Further up section, these rocks are intruded by thick sills of MORB-like tholeiitic gabbro. The lower contact of one of these sills is exposed in the northern portion of this outcrop and shows a thick chilled margin.

Proceed north (back toward PR304) on the logging road for 300 m to a south-facing outcrop just off the left (west) shoulder of the road, near the base of a low outcrop ridge.

Stop 2 (319689mE, 5655519mN):
Bidou assemblage, Rainy Lake Road unit

This outcrop shows a 25 m thick section of well-stratified felsic epiclastic rocks at the top of the medial section of the Rainy Lake Road unit (Figure 3). These rocks consist of thick to thin-bedded pebbly volcanic sandstone, with subordinate interbeds of laminated sulphidic mudstone and heterolithic pebble conglomerate. Planar sandstone beds vary from massive to normal size-graded. Local scours indicate that these rocks are upright. A sharp depositional contact separates these epiclastic rocks from the overlying pillowed to massive flows of MORB-like tholeiitic basalt that dominate the upper section of the basin-fill.

A crudely-graded layer of felsic volcanic conglomerate in the middle portion of this section was sampled for U-Pb geochronological analysis to constrain the timing of basin infilling. This layer is 3.0 m thick and is marked at the base by a sharp undulatory contact that locally cuts down through an underlying bed of black mudstone. The layer exhibits reverse size-grading at the base and a diffuse normal size-grading in the upper portion. The conglomerate is matrix supported and poorly sorted, and contains angular to subrounded clasts of dark grey feldspar-phyric dacite, with subordinate clasts of porphyritic andesite, aphyric and quartz-phyric rhyolite, felsic tuff, amygdaloidal basalt, mudstone and solid sulphide. The sulphide clasts are subangular to subrounded and consist mainly of massive, fine-grained pyrrhotite, with minor chalcopyrite. This conglomerate represents a proximal subaqueous debris flow that may have been shed off a fault-scarp in the footwall of the postulated G_1 subsidence structure. The sulphide clasts are suggestive of coeval exhalative activity along this structure.

U-Pb (TIMS) analyses of single detrital zircons yielded one concordant analysis with a $^{207}Pb/^{206}Pb$ age of 2747.4 ±5.7 Ma, and one near-concordant (–0.5%) analysis with an age of 2727.1 ±0.8 Ma. Two other single zircon crystals gave slightly discordant analyses with ages of 2731.3 ±0.4 Ma (1.1% discordant) and 2727.4 ±2.8 Ma (3.2% discordant), whereas a multigrain fraction (5 grains) gave a slightly discordant analysis (2.6%) with an age of 2736.8 ±1.3 Ma. The essentially identical ca. 2727 Ma $^{207}Pb/^{206}Pb$ ages of two of the single-zircon analyses give a weighted-average age of 2727.1 ±1.5 Ma, which is interpreted to represent the maximum depositional age. In keeping with the heterolithic nature of the conglomerate, the slightly older ages are interpreted to reflect slightly older detrital or inherited components, perhaps derived from the IL unit in the footwall of the postulated subsidence structure.

Return to PR304. Drive 2.5 km west (back toward Bissett) on PR304 to an unmarked turnoff leading to a large rock quarry on the right (north) side of the road. Turn right off PR304 and park in front of the large boulders blocking the entrance to the quarry.

Stop 3 (317247mE, 5656681mN):
Bidou assemblage, Round Lake unit

The quarry in this location is situated along the south margin of the Wanipigow Shear Zone (WSZ) and exposes felsic epiclastic rocks in the Round Lake unit of the Bidou assemblage (Figure 3). In the walls of the quarry, thin intervals of planar-bedded volcanic sandstone can be seen to separate 1–3 m thick layers of heterolithic, poorly sorted, pebble to cobble volcanic conglomerate. Bedding dips steeply north and normally-graded sandstone beds and rare scours indicate these rocks are upright. Aspect ratios of deformed clasts in horizontal vs. vertical exposures define a shallowly east-plunging stretching lineation, which is interpreted as a composite fabric formed via reorientation and attenuation of the regional L_3 shape fabric (Figure 8) during progressive non-coaxial shear (G_4 and G_5) along the south margin of the WSZ. Vertical

outcrop surfaces show a somewhat less pronounced planar shape fabric (composite S_3-S_4-S_5) defined by flattened clasts that parallels a penetrative sericite-chlorite foliation. Seams of mylonite and ultramylonite are conspicuous in the clean outcrop surface on the eastern flank of the quarry and are interpreted as G_5 structures resulting from transcurrent shear deformation. Shear bands, porphyroclast systems and asymmetric boudins in these outcrops indicate dextral shear. Antithetic shear bands may indicate a component of synkinematic zone-normal shortening.

Return to PR304. Drive 300 m west (back toward Bissett) on PR304 to an unmarked turnoff leading to a gravel pit on the right (north) side of the road. Turn right and park in the bottom of the pit.

Stop 4 (316965mE, 5656619mN):
Bidou assemblage, Round Lake unit

This outcrop consists of heterolithic volcanic conglomerate of the Round Lake unit, at approximately the same stratigraphic position as the previous outcrop (Figure 3); however, significantly higher finite strain in this location has all but obliterated the primary clastic texture of the rock. Aspect ratios of deformed clasts in the horizontal outcrop surface locally exceed 100:1 (X:Z), which is anomalous as compared to other coarse clastic rocks in the Rice Lake area. The very high apparent finite strain recorded in these rocks may be a consequence of their location near the confluence of the Wanipigow and Normandy Creek shear zones (Figure 3).

Return to PR304. Drive back through Bissett on PR304 to the intersection with Quesnel Lake road (5.7 km from the Post Office in Bissett). Turn left (south) and proceed along the Quesnel Lake road for 6.6 km to the short causeway at the outlet of Red Rice Lake (marked by small wooden sign on right side of road). Proceed 100 m further south along Quesnel Lake road to an unmarked turnoff to a partially overgrown bush-road on the left (east) side of the road. Park vehicles at the turnoff.

Walk east along the bush road for 550 m to a fork in the road. Staying left, follow the orange flagging tape in a generally northwesterly direction along an overgrown skidder trail to a low outcrop that is elongate in the east-west direction (approximately 800 m walking distance).

Stop 5 (311477mE, 5653788mN):
San Antonio assemblage

As originally described by Stockwell (1938), this outcrop shows the intact unconformable contact between the San Antonio assemblage and underlying intermediate volcaniclastic rocks of the Independence Lake unit of the Bidou assemblage (Figures 3, 5). The east end of the outcrop shows crudely stratified tuff breccia crosscut by an andesite dike. The tuff breccia contains three distinct generations of planar fabric, which correspond to the regionally-pervasive S_3, S_4 and S_5 fabrics. The S_3 fabric trends northwest, slightly clockwise from S_0, and is defined by flattened clasts and a continuous chlorite foliation in the matrix. This fabric is overprinted by a finely-spaced crenulation cleavage (S_4) that trends west-northwest and is well-preserved in the flattened clasts, where it clearly transects the X-axes at shallow counter-clockwise angles. Both of these fabrics are overprinted by a spaced shear-band cleavage (S_5) that trends north-northwest and has a dextral sense of asymmetry. A well-developed north-trending crenulation cleavage in the andesite dike may correspond to the regional S_6 fabric or, alternatively, the S_5 fabric refracted through the dike.

The base of the San Antonio assemblage is marked by a 1–1.5 m thick layer of pebble-cobble conglomerate composed mostly of intermediate volcanic detritus of apparently local derivation, with scattered pebbles of vein quartz. Near the top, the conglomerate contains interbeds of quartz arenite up to 1 m thick. These rocks are overlain to the west by medium-grained quartz arenite that contains well-developed crossbeds and local ripple cross laminations; bedding here dips steeply southwest or northeast (overturned), markedly oblique to stratification in the underlying rocks. Further up section, at the western extent of the outcrop, coarser-grained pebbly arenite contains spectacular trough crossbeds. Deformation fabrics are not well-developed in this portion of the outcrop, perhaps on account of the relatively 'clean' nature of the quartz arenites.

Return to Quesnel Lake road. Drive south for 500 m along the Quesnel Lake road to a sharp left turn at the southeast corner of Red Rice Lake. Park in the cleared area on the right side of the road at the turn.

Stop 6 (311100mE, 5652607mN):
San Antonio assemblage

This outcrop shows tonalitic conglomerate and sandstone at the base of the San Antonio assemblage, on the upright southern limb of the G_3 Gold Creek syncline. The outcrop on the south side of the trail leading to the lake consists of massive monomictic conglomerate composed of closely-packed, subangular to rounded, cobbles and boulders of medium-grained, equigranular tonalite in a matrix of pebbly feldspathic wacke and rare mudstone. Erosion and transport of tonalite, as opposed to in-situ brecciation, is indicated by aplite dikes in some clasts that cannot be traced through the matrix or into adjacent clasts. The easternmost tip of this outcrop may expose the unconformable contact with underlying volcaniclastic rocks of the Bidou assemblage, which appear to be cut by a pale pink felsic dike. The conglomerate generally coarsens toward the west, where it is exposed in a series of outcrops that extend up to the contact of the large tonalite-granodiorite pluton. Boulders in these outcrops range up to several metres across. Further west, a nonconformable contact between the conglomerate and underlying pluton is exposed at a classical (and poorly accessible) locality described by Stockwell (1938) and Davies (1963).

The outcrop on the north side of the trail leading to the lake consists of a heterogeneously transposed section of interbedded medium- to very coarse grained, pebbly feldspathic wacke (tonalite grit), pebble conglomerate and sericitic mudstone. Lenticular packets of intact, moderately northwest-dipping bedding are separated by northwest-trending zones of intense transposition and foliation development. Within these packets, a spaced crenulation cleavage is oriented nearly orthogonal to bedding and overprints an early bedding-parallel (S_2?) foliation. The transposition fabric and crenulation cleavage (S_3) are axial planar to the G_3 Gold Creek syncline, which plunges shallowly to the northwest, and are transected at a shallow counter-clockwise angle by the S_4 crenulation cleavage. The upper surface of the outcrop is oriented nearly parallel to the F_3 enveloping surface, which partially obscures the bedded aspect of these rocks.

Return to PR304. Turn left and proceed 100 m west on PR304 to an unmarked turnoff on the right (north) side of the road. Turn right and drive north for 100 m to the low washed outcrop on the right (east) side of the road, approximately 50 m south of the entrance to the rock quarry.

Stop 7 (307249mE, 5657456mN):
San Antonio assemblage

This outcrop shows pebbly quartz arenite in the upper portion of the San Antonio assemblage, near the hinge of the G_3 Horseshoe Lake anticline. Here, the quartz arenites contain large-scale trough crossbeds, with bottomsets locally defined by diffuse pebble-lag deposits. The prominent lag deposit in the central portion of the outcrop consists of sericitized clasts of intermediate volcanic and plutonic material. Flattened pebbles and a penetrative sericite foliation define the S_3 planar fabric in this outcrop, which deviates from the regional northwest trend on account of refraction through the overturned limb of the anticline. This fabric is overprinted at a shallow counter-clockwise angle by a finely-spaced S_4 crenulation cleavage. The long axes of the flattened pebbles accentuate the near-orthogonal angular relationship between bedding and S_3, in keeping with the structural location near the hinge of the macroscopic G_3 anticline. Immediately west of this location, the San Antonio assemblage lies in contact with intermediate volcaniclastic rocks of the Bidou assemblage (Gold Creek unit), which likewise face west on the regional S_3 fabric. This older-over-younger map pattern is interpreted to result from imbrication of the Bidou and San Antonio assemblages by G_2 thrust faults.

Return to PR304. Drive west for 4.5 km to the turnoff to Currie's Landing on the right (north) side of the road (marked by small wooden sign and bright yellow "Designated Route R" sign). Proceed 1.1 km northwest along the Currie's Landing road to the turnoff of the Pointer Lake forestry access road on the right. Turn right (east) and drive for 2.4 km to the bridge over the Wanipigow River. Park 100 m north of the bridge, on the right (east) side of the road (at orange flagging). Walk east approximately 50 m to a low bush outcrop.

Stop 8 (305114mE, 5661278mN):
San Antonio assemblage

This outcrop is situated along the main trace of the Wanipigow Shear Zone and shows a spectacular example of strongly-deformed polymictic conglomerate of the San Antonio assemblage. The conglomerate is clast-supported, unsorted and contains minor interbeds of feldspathic wacke. Well-rounded and roughly equant clasts of more competent tonalite contrast with strongly flattened clasts of less competent intermediate to felsic volcanic material. The tonalite clasts typically exhibit well-developed asymmetric (σ-type) tails, with local synthetic and/or antithetic shear factures or quartz-filled extension fractures. Gentle to tight Z-folds, which are a characteristic feature of the core of the Wanipigow Shear Zone, plunge shallowly east in this location.

U-Pb analyses of detrital zircons from a sample of greywacke collected just west of the bridge over the Wanipigow River define two distinct age clusters at 2705–2747 Ma and 2938–3006 Ma, which is typical of the young fluvial-alluvial clastic successions in the Rice Lake belt.

Return to PR304. End of field trip.

References

Anderson, S.D. 2004: Preliminary results and economic significance of geological mapping and structural analysis in the Rice Lake area, central Rice Lake greenstone belt, Manitoba (NTS 52M4 and 52L13); *in* Report of Activities 2004, Manitoba Industry, Economic Development and Mines, Manitoba Geological Survey, p. 216–231.

Anderson, S.D. 2005: Geology and structure of the Rice Lake area, Rice Lake greenstone belt, Manitoba (part of NTS 52M04 and 52L13); Manitoba Industry, Economic Development and Mines, Manitoba Geological Survey, Preliminary Map PMAP2005-1, scale 1:20 000.

Anderson, S.D. 2008: Geology of the Rice Lake area, Rice Lake greenstone belt, southeastern Manitoba (parts of NTS 52L13, 52M4); Manitoba Science, Technology, Energy and Mines, Manitoba Geological Survey, Geoscientific Report GR2008-1, 97 p.

Bailes, A.H. 1971: Geology and geochemistry of the Pilot-Smuggler shear zone, Rice Lake region, southeastern Manitoba; *in* Geology and Geophysics of the Rice Lake Region, Southeastern Manitoba (Project Pioneer), W.D. McRitchie and W. Weber (ed.), Manitoba Department of Mines and Natural Resources, Mines Branch, Publication 71-1, p. 299–312.

Bailes, A.H. 1998: Geochemical sampling of the Bidou Lake subgroup of the Rice Lake greenstone belt; *in* Report of Activities 1998, Manitoba Energy and Mines, Geological Services, p. 144–150.

Bailes, A.H. and Percival, J.A. 2000: Geology and structure of the North Caribou Terrane–Uchi Subprovince boundary in eastern Manitoba, with emphasis on volcanic and volcaniclastic rocks of the Black Island assemblage; *in* Report of Activities 2000, Manitoba Industry, Trade and Mines, Manitoba Geological Survey, p. 161–174.

Bailes, A.H. and Percival, J.A. 2005: Geology of the Black Island area, Lake Winnipeg, Manitoba (parts of NTS 62P1, 7 and 8); Manitoba Industry, Economic Development and Mines, Manitoba Geological Survey, Geoscientific Report GR2005-2, 33 p.

Bailes, A.H., Percival, J.A., Corkery, M.T., McNicoll, V.J., Tomlinson, K.Y., Sasseville, C., Rogers, N., Whalen, J.B. and Stone, D. 2003: Geology and tectonostratigraphic assemblages, West Uchi map area, Manitoba and Ontario; Manitoba Geological Survey, Open File OF2003-1, 1:250 000 scale with marginal notes.

Barrie, C.T., Ludden, J.M. and Green, T.H. 1993: Geochemistry of volcanic rocks associated with Cu-Zn and Ni-Cu deposits in the Abitibi Subprovince; Economic Geology, v. 88, p. 1341–1358.

Breaks, F.W. 1991: English River Subprovince; *in* Geology of Ontario, P.C. Thurston, H.R. Williams, R.H. Sutcliffe and G.M. Stott, (ed.), Ontario Geological Survey, Special Volume 4, Part 1, p. 239–277.

Bruhn, R.L., Parry, W.T., Yonkee, W.A. and Thompson, T. 1994: Fracturing and hydrothermal alteration in normal fault zones; Pure and Applied Geophysics, v. 142, p. 609–644.

Card, K.D. 1990: A review of the Superior Province of the Canadian Shield, a product of Archean accretion; Precambrian Research, v. 48, p. 99–156.

Card, K.D. and Ciesielski, A. 1986: Subdivisions of the Superior Province of the Canadian Shield; Geoscience Canada, v. 13, p. 5–13.

Corfu, F., Stott, G.M. and Breaks, F.W. 1995: U-Pb geochronology and evolution of the English River Subprovince, an Archean low P-high T metasedimentary belt in the Superior Province; Tectonics, v. 14, p. 1220–1233.

Davies, J.F. 1953: Geology and gold deposits of southern Rice Lake area; Manitoba Department of Mines and Natural Resources, Mines Branch, Publication 52-1, 41 p.

Davies, J.F. 1963: Geology and gold deposits of the Rice Lake–Wanipigow River area, Manitoba; Ph.D. thesis, University of Toronto, Ontario, 142 p.

Davis, D.W. 1994: Report on the geochronology of rocks from the Rice Lake belt, Manitoba; Royal Ontario Museum, Geology Department, Toronto, Ontario, unpublished report.

Davis, D.W. 1996: Provenance and depositional age constraints on sedimentation in the Western Superior Transect area from U-Pb ages of zircons; *in* LITHOPROBE Western Superior Transect, Report of Second Annual Workshop, R.M. Harrap and H. Helmstaedt (ed.), LITHOPROBE Secretariat, University of British Columbia, Report 53, p. 18–23.

Davis, D.W. 1998: Speculations on the formation and crustal structure of the Superior province from U-Pb geochronology; *in* Western Superior LITHOPROBE Transect, Fourth Annual Workshop, R.M. Harrap and H.H. Helmstaedt (ed.), LITHOPROBE Secretariat, University of British Columbia, Report 65, p. 21–28.

Defant, M.J. and Drummond, M.S. 1990: Derivation of some modern arc magmas by melting of young subducted lithosphere; Nature, v. 347, p. 662–665.

Ermanovics, I.F. and Wanless, R.K. 1983: Isotopic age studies and tectonic interpretation of Superior Province in Manitoba; Geological Survey of Canada, Paper 82-12, 22 p.

George, P.T. 2006: Mineral resource and mineral reserve estimates as of December 1, 2006, Rice Lake project, Rice Lake greenstone belt, Bissett, Manitoba, Canada, for San Gold Corporation; A.C.A. Howe International Ltd., Report 902, 160 p.

Hoffman, P.F. 1989: Precambrian geology and tectonic history of North America; *in* The Geology of North America – an overview, A.W. Bally and A.R. Palmer (ed.), Geological Society of America, The Geology of North America, v. A, p. 447–512.

Hollings, P., Wyman, D. and Kerrich, R. 1999: Komatiite-basalt-rhyolite volcanic associations in northern Superior Province greenstone belts: significance of plume-arc interaction in the generation of the proto continental Superior Province; Lithos, v. 46, p. 137–161.

Krogh, T.E., Ermanovics, I.F. and Davis, G.L. 1974: Two episodes of metamorphism and deformation in the Archean rocks of the Canadian shield; *in* Carnegie Institution of Washington, Geophysical Laboratory Yearbook, 1974, v. 73, p. 573–575.

Langford, F.F. and Morin, J.A. 1976: The development of the Superior Province of northwestern Ontario by merging island arcs; American Journal of Science, v. 276, p. 1023–1034.

Lau, M.H.S. and Brisbin, W.C. 1996: Structural geology of the San Antonio mine, Bissett, Manitoba; Geological Survey of Canada, Open File 1699, 65 p.

Lemkow, D.R., Sanborn-Barrie, M., Bailes, A.H., Percival, J.A., Rogers, N., Skulski, T., Anderson, S.D., Tomlinson, K.Y., McNicoll, V., Parker, J.R., Whalen, J.B., Hollings, P. and Young, M. 2006: GIS compilation of geology and tectonostratigraphic assemblages, western Uchi Subprovince, western Superior Province, Ontario and Manitoba; Manitoba Geological Survey, Open File OF2006-30, CD-ROM.

Lesher, C.M., Goodwin, A.M., Campbell, I.H. and Gorton, M.P. 1986: Trace-element geochemistry of ore-associated and barren, felsic metavolcanic rocks in the Superior Province, Canada; Canadian Journal of Earth Sciences, v. 23, p. 222–237.

Martin, H., Smithies, R.H., Rapp, R., Moyen, J-F. and Champion, D. 2005: An overview of adakite, tonalite-trondhjemite-granodiorite (TTG), and sanukitoid: relationships and some implications for crustal evolution; Lithos, v. 79, p. 1–24.

McRitchie, W.D. and Weber, W. 1971: Metamorphism and deformation in the Manigotagan Gneissic Belt, south-eastern Manitoba; *in* Geology and Geophysics of the Rice Lake Region, Southeastern Manitoba (Project Pioneer), W.D. McRitchie and W. Weber (ed.), Manitoba Department of Mines and Natural Resources, Mines Branch, Publication 71-1, p. 235–284, and accompanying Maps 69-1 to 4.

Pan, Y., Therens, C. and Ansdell, K. 1998: Geochemistry of mafic-ultramafic rocks from the Werner–Gordon Lake area: back-arc origin for the English River subprovince?; *in* Western Superior LITHOPROBE Transect, Fourth Annual Workshop, R.M. Harrap and H.H. Helmstaedt (ed.), LITHOPROBE Secretariat, University of British Columbia, Report 65, p. 29–34.

Pearce, J.A. and Peate, D.W. 1995: Tectonic implications of the composition of volcanic arc magmas; Annual Review of Earth and Planetary Sciences, v. 23, p. 251–285.

Percival, J.A., Bailes, A. and McNicoll, V. 2002: Mesoarchean breakup, Neoarchean accretion in the western Superior craton, Lake Winnipeg, Canada; Geological Association of Canada–Mineralogical Association of Canada, Joint Annual Meeting, May 30–June 2, 2002, Saskatoon, Saskatchewan, Field Trip B3 Guidebook, 42 p.

Percival, J.A., Sanborn-Barrie, M., Skulski, T., Stott, G.M., Helmstaedt, H. and White, D.J. 2006a: Tectonic evolution of the western Superior Province from NATMAP and LITHOPROBE studies; Canadian Journal of Earth Sciences, v. 43, p. 1085–1117.

Percival, J.A., McNicoll, V. and Bailes, A.H. 2006b: Strike-slip juxtaposition of ca. 2.72 Ga juvenile arc and >2.98 Ga continent margin sequences and its implications for Archean terrane accretion, western Superior Province, Canada; Canadian Journal of Earth Sciences, v. 43, p. 895–927.

Poulsen, K.H., Ames, D.E., Lau, S. and Brisbin, W.C. 1986: Preliminary report on the structural setting of gold in the Rice Lake area, Uchi Subprovince, southeastern Manitoba; *in* Current Research, Part B, Geological Survey of Canada, Paper 86-1B, p. 213–221.

Poulsen, K.H., Weber, W., Brommecker, R. and Seneshen, D.N. 1996: Lithostratigraphic assembly and structural setting of gold mineralization in the eastern Rice Lake greenstone belt, Manitoba; Geological Association of Canada–Mineralogical Association of Canada, Joint Annual Meeting, May 27–29, 1996, Winnipeg, Manitoba, Field Trip A4 Guidebook, 106 p.

Richards, J.P. and Kerrich, R. 2007: Adakite-like rocks: their diverse origins and questionable role in metallogenesis; Economic Geology, v. 102, p. 537–576.

Sanborn-Barrie, M., Skulski, T. and Parker, J. 2001: Three hundred million years of tectonic history recorded by the Red Lake greenstone belt, Ontario; Geological Survey of Canada, Current Research 2001-C19, 19 p.

Sasseville, C., Tomlinson, K.Y., Hynes, A. and McNicoll, V. 2006: Stratigraphy, structure, and geochronology of the 3.0–2.7 Ga Wallace Lake greenstone belt, western Superior Province, southeast Manitoba, Canada; Canadian Journal of Earth Sciences, v. 43, p. 929–945.

Shirey, S.B. and Hanson, G.N. 1984: Mantle derived Archaean monzodiorites and trachyandesites; Nature, v. 310, p. 222–224.

Sinton, J.M. and Fryer, P. 1987: Mariana Trough lavas from 18°N: implications for the origin of back arc basin basalts; Journal of Geophysical Research, v. 92, no. B12, p. 12782–12802.

Skulski, T., Corkery, M.T., Stone, D., Whalen, J.B. and Stern, R.A. 2000: Geological and geochronological investigations in the Stull Lake–Edmund Lake greenstone belt and granitoid rocks of the northwestern

Superior Province; *in* Report of Activities 2000, Manitoba Industry, Trade and Mines, Manitoba Geological Survey, p. 117–128.

Stern, R. 1989: Petrogenesis of the Archaean Sanukitoid Suite; State University at Stony Brook, New York, 275 p.

Stern, R.A., Hanson, G.N. and Shirey, S.B. 1989: Petrogenesis of mantle-derived, LILE-enriched Archean monzodiorites and trachyandesites (sanukitoids) in southwestern Superior Province; Canadian Journal of Earth Sciences, v. 26, p. 1688–1712.

Stockwell, C.H. 1938: Rice Lake–Gold Lake area, southern Manitoba; Canada Department of Mines and Resources, Geological Survey, Memoir 210, 79 p.

Stott, G.M. and Corfu, F. 1991: Uchi Subprovince; *in* Geology of Ontario, P.C. Thurston, H.R. Williams, R.H. Sutcliffe and G.M. Stott, (ed.), Ontario Geological Survey, Special Volume 4, Part 1, p. 145–236.

Sun, S.-S. and McDonough, W.F. 1989: Chemical and isotopic systematics of oceanic basalts: implications for mantle composition and processes; *in* Magmatism in the Ocean Basins, A.D. Saunders and M.J. Norry, (ed.), Geological Society of London, Special Publication 42, p. 313–345.

Thurston, P.C., Osmani, I.A. and Stone, D. 1991: Northwestern Superior Province: review and terrane analysis; *in* Geology of Ontario, P.C. Thurston, H.R. Williams, R.H. Sutcliffe and G.M. Stott (ed.), Ontario Geological Survey, Special Volume 4, Part 1, p. 81–142.

Tobisch, O.T. and Paterson, S.R. 1988: Analysis and interpretation of composite foliations in areas of progressive deformation; Journal of Structural Geology, v. 10, p. 745–754.

Turek, A. and Weber, W. 1991: New U-Pb zircon ages from the Rice Lake area: evidence for 3 Ga crust; *in* Report of Activities 1991, Manitoba Energy and Mines, Minerals Division, p. 53–55.

Turek, A., Keller, R., Van Schmus, W.R. and Weber, W. 1989: U-Pb zircon ages for the Rice Lake area, southeastern Manitoba; Canadian Journal of Earth Sciences, v. 26, p. 23–30.

Weber, W. 1971: The evolution of the Rice Lake – Gem Lake greenstone belt, southeastern Manitoba; *in* Geoscience Studies in Manitoba, A.C. Turnock (ed.), Geological Association of Canada, Special Paper, v. 9, p. 97–103.

Whalen, J.B., Percival, J.A., McNicoll, V.J. and Longstaffe, F.J. 2003: Intra-oceanic production of continental crust in a Th-depleted ca. 3.0 Ga arc complex, western Superior Province, Canada; Contributions to Mineralogy and Petrology, v. 146, p. 78–99.

Williams, H.R., Stott, G.M., Thurston, P.C., Sutcliffe, R.H., Bennett, G., Easton, R.M. and Armstrong, D.K. 1992: Tectonic evolution of Ontario: summary and synthesis; *in* Geology of Ontario, P.C. Thurston, H.R. Williams, R.H. Sutcliffe and G.M. Stott (ed.), Ontario Geological Survey, Special Volume 4, Part 2, p. 1255–1332.

Figure captions

Figure 1: Regional geological setting of the Rice Lake belt in the western Uchi Subprovince (modified after Lemkow et al., 2006). Abbreviations: MSZ, Manigotagan Shear Zone; SL–LSJF, Sydney Lake–Lake St. Joseph Fault; WSZ, Wanipigow Shear Zone.

Figure 2: Simplified geology of the Rice Lake belt, showing the principal lithotectonic assemblages, major gold deposits and location of the field trip area. Abbreviations: BLSZ, Beresford Lake Shear Zone; HR, Hole River assemblage; LB, Little Beaver assemblage; L-S, Lewis-Storey assemblage; M, Manigotagan assemblage; MSZ, Manigotagan Shear Zone; RRP, Ross River pluton; S, Siderock assemblage; W, Wallace assemblage; WSZ, Wanipigow Shear Zone.

Figure 3: Geology of the Rice Lake area, after Map GR2008-1-1 (Anderson, 2008), showing the locations of the field trip stops (S-1 to S-8). The locations of the Independence Lake (IL), Rainy Lake road (RLR), Townsite (TS) and Round Lake (RL) units are shown for reference. Abbreviations: GCSZ, Gold Creek Shear Zone; NCSZ, Normandy Creek Shear Zone; RRLSZ, Red Rice Lake Shear Zone; WSZ, Wanipigow Shear Zone (indicated by hachured pattern).

Figure 4: Schematic lithostratigraphy of the Rice Lake section of the Bidou assemblage (vertical section, looking toward present-day north). For simplicity, the geology north of the Wanipigow Shear Zone and west of the San Antonio assemblage is excluded. The numbered ellipses correspond to the map unit numbers in GR2008-1 (Anderson, 2008). The heavy grey dashed line indicates the approximate location of the postulated subsidence structure east of Rice Lake. The thickness of the exhalite and solid sulphide horizon in the RLR unit is exaggerated. Abbreviations: IL, Independence Lake unit; RL, Round Lake unit; RLR, Rainy Lake road unit; TS, Townsite unit.

Figure 5: Detailed outcrop map showing the angular unconformity at the base of the San Antonio assemblage. This locality, 600 m northeast of Red Rice Lake, was originally mapped and described by Stockwell (1938).

Figure 6: Normal mid-ocean-ridge basalt (NMORB)- and primitive mantle-normalized extended-element plots for mafic volcanic and plutonic rocks from the Rice Lake area. Normalizing values are from Sun and McDonough (1989).

Figure 7: Chondrite- (a) and primitive mantle-normalized (b) extended-element plots for felsic volcanic and plutonic rocks from the Rice Lake area. Normalizing values are from Sun and McDonough (1989).

Figure 8: Schematic map showing the trends of the S_3 and L_3 fabrics (dashed lines) and the plunge of the L_3 lineation (contours) in the Rice Lake area. The systematic change in trend and plunge of the L_3 lineation along the margin of the Wanipigow Shear Zone was originally described by Poulsen et al. (1986). Abbreviations: RLM, Rice Lake mine (A-shaft); SG-1, SG-1 mine portal.

Figure 9: Schematic block diagrams illustrating the structural evolution of the Rice Lake area. Not depicted is the D_1 deformation, which is interpreted to be associated with extensional faulting in the Bidou assemblage prior to D_2 tilting. Abbreviations: BA, Bidou assemblage; NCSZ, Normandy Creek Shear Zone; SAA, San Antonio assemblage; WSZ, Wanipigow Shear Zone.

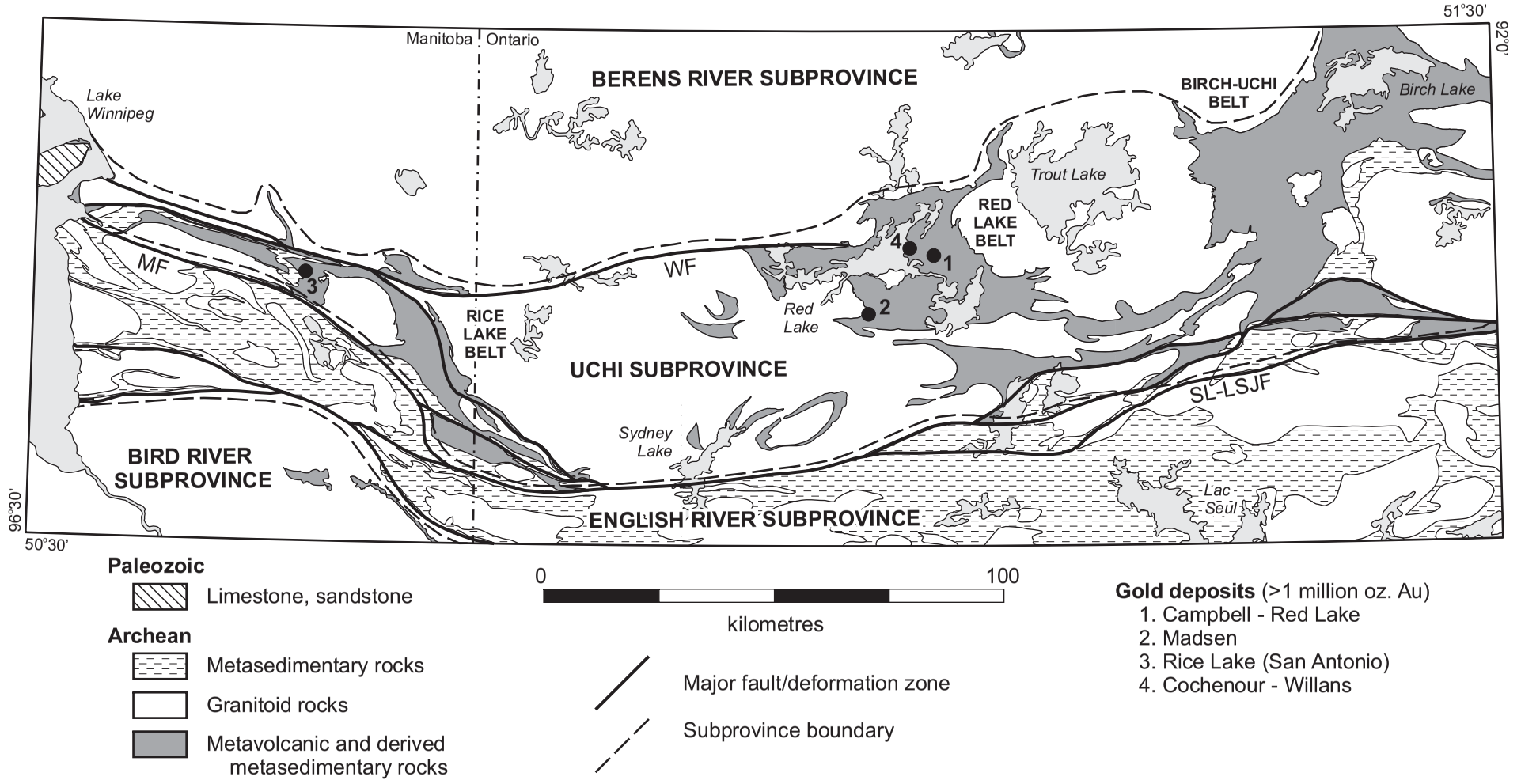
51°30'
92°0'
96°30'
50°30'
Manitoba
Ontario
Lake Winnipeg
BERENS RIVER SUBPROVINCE
BIRCH-UCHI BELT
Birch Lake
Trout Lake
RED LAKE BELT
MF
WF
RICE LAKE BELT
Red Lake
UCHI SUBPROVINCE
SL-LSJF
Sydney Lake
BIRD RIVER SUBPROVINCE
Lac Seul
ENGLISH RIVER SUBPROVINCE
1
2
3
4
Paleozoic
Limestone, sandstone
Archean
Metasedimentary rocks
Granitoid rocks
Metavolcanic and derived metasedimentary rocks
0
100
kilometres
Major fault/deformation zone
Subprovince boundary
Gold deposits (>1 million oz. Au)
1. Campbell - Red Lake
2. Madsen
3. Rice Lake (San Antonio)
4. Cochenour - Willans

Figure 1

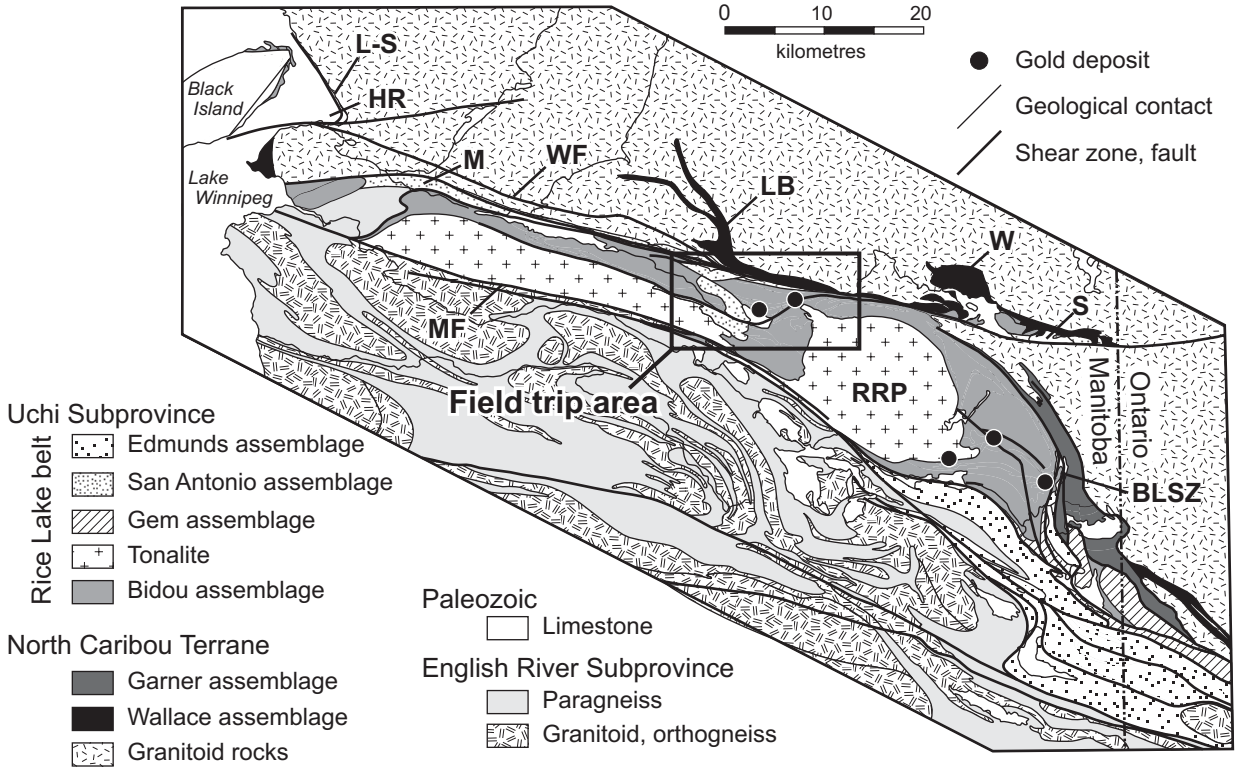
0
10
20
kilometres
Gold deposit
Geological contact
Shear zone, fault
L-S
HR
Black Island
Lake Winnipeg
M
WF
LB
W
S
MF
Field trip area
RRP
Manitoba
Ontario
BLSZ
Uchi Subprovince
Rice Lake belt
Edmunds assemblage
San Antonio assemblage
Gem assemblage
Tonalite
Bidou assemblage
North Caribou Terrane
Garner assemblage
Wallace assemblage
Granitoid rocks
Paleozoic
Limestone
English River Subprovince
Paragneiss
Granitoid, orthogneiss

Figure 2

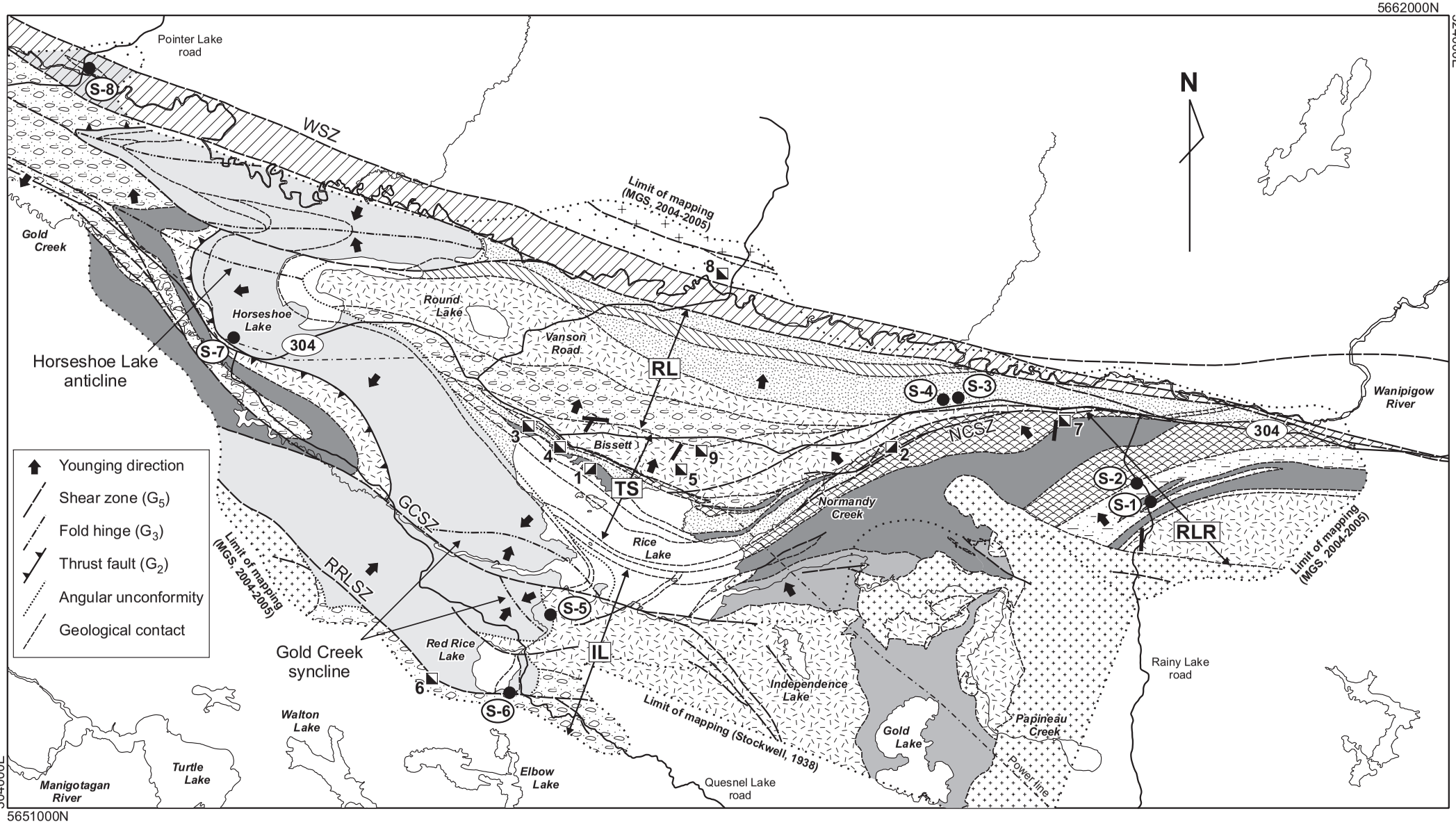

San Antonio assemblage

- Arenite, conglomerate, greywacke

Bidou assemblage

- Quartz-feldspar porphyry
- Tonalite-granodiorite
- Gabbro
- Diabase, basalt tuff (sanukitoid affinity)
- Basalt flows (pillowed and massive)
- Greywacke, mudstone, chert, basalt, felsic epiclastic rocks
- Felsic epiclastic rocks
- Volcanic conglomerate (heterolithic)
- Flows and volcaniclastic rocks (andesite)
- Volcaniclastic rocks (andesite-dacite)

0 — 5 kilometres

S-1 ● 2009 Field trip stops

North Caribou Terrane

- Tonalite-granodiorite
- Psammite, semipelite, gabbro, iron formation

- Producing mines:
  1. Rice Lake mine
  2. San Gold #1
- Deposits/prospects:
  3. Cartwright
  4. Gabrielle
  5. Gold Standard
  6. Packsack
  7. San Gold #3
  8. Vanson
  9. Wingold

Figure 3

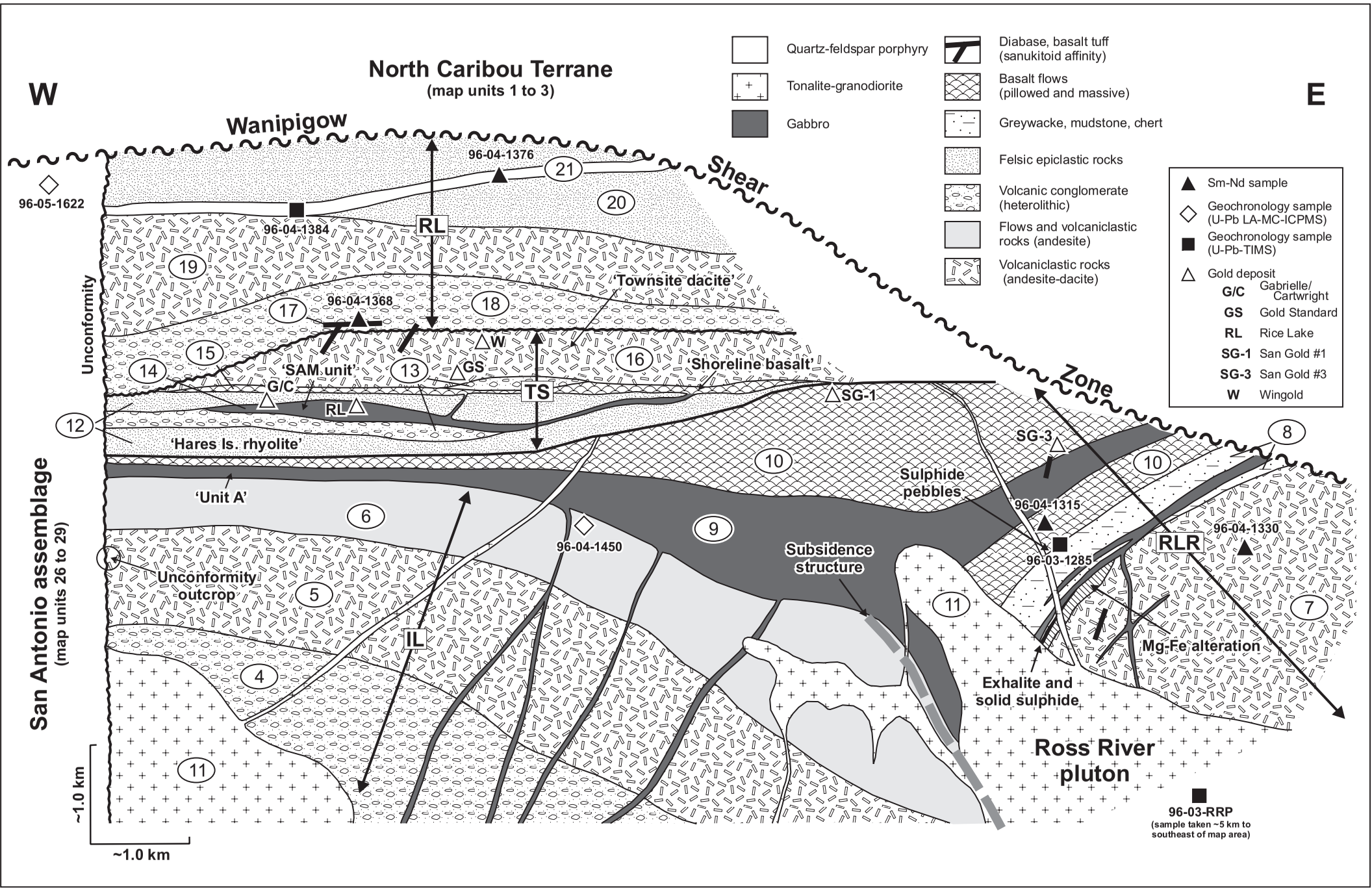
W
E
North Caribou Terrane
(map units 1 to 3)
Wanipigow
Shear
Zone
Unconformity
San Antonio assemblage
(map units 26 to 29)
Quartz-feldspar porphyry
Tonalite-granodiorite
Gabbro
Diabase, basalt tuff
(sanukitoid affinity)
Basalt flows
(pillowed and massive)
Greywacke, mudstone, chert
Felsic epiclastic rocks
Volcanic conglomerate
(heterolithic)
Flows and volcaniclastic
rocks (andesite)
Volcaniclastic rocks
(andesite-dacite)
Sm-Nd sample
Geochronology sample
(U-Pb LA-MC-ICPMS)
Geochronology sample
(U-Pb-TIMS)
Gold deposit
G/C Gabrielle/
Cartwright
GS Gold Standard
RL Rice Lake
SG-1 San Gold #1
SG-3 San Gold #3
W Wingold
96-05-1622
96-04-1384
96-04-1376
96-04-1368
96-04-1450
96-04-1315
96-03-1285
96-04-1330
96-03-RRP
(sample taken ~5 km to
southeast of map area)
RL
TS
IL
RLR
'Townsite dacite'
'SAM unit'
'Shoreline basalt'
'Hares Is. rhyolite'
'Unit A'
Sulphide
pebbles
Subsidence
structure
Unconformity
outcrop
Exhalite and
solid sulphide
Mg-Fe alteration
Ross River
pluton
~1.0 km
~1.0 km

Figure 4

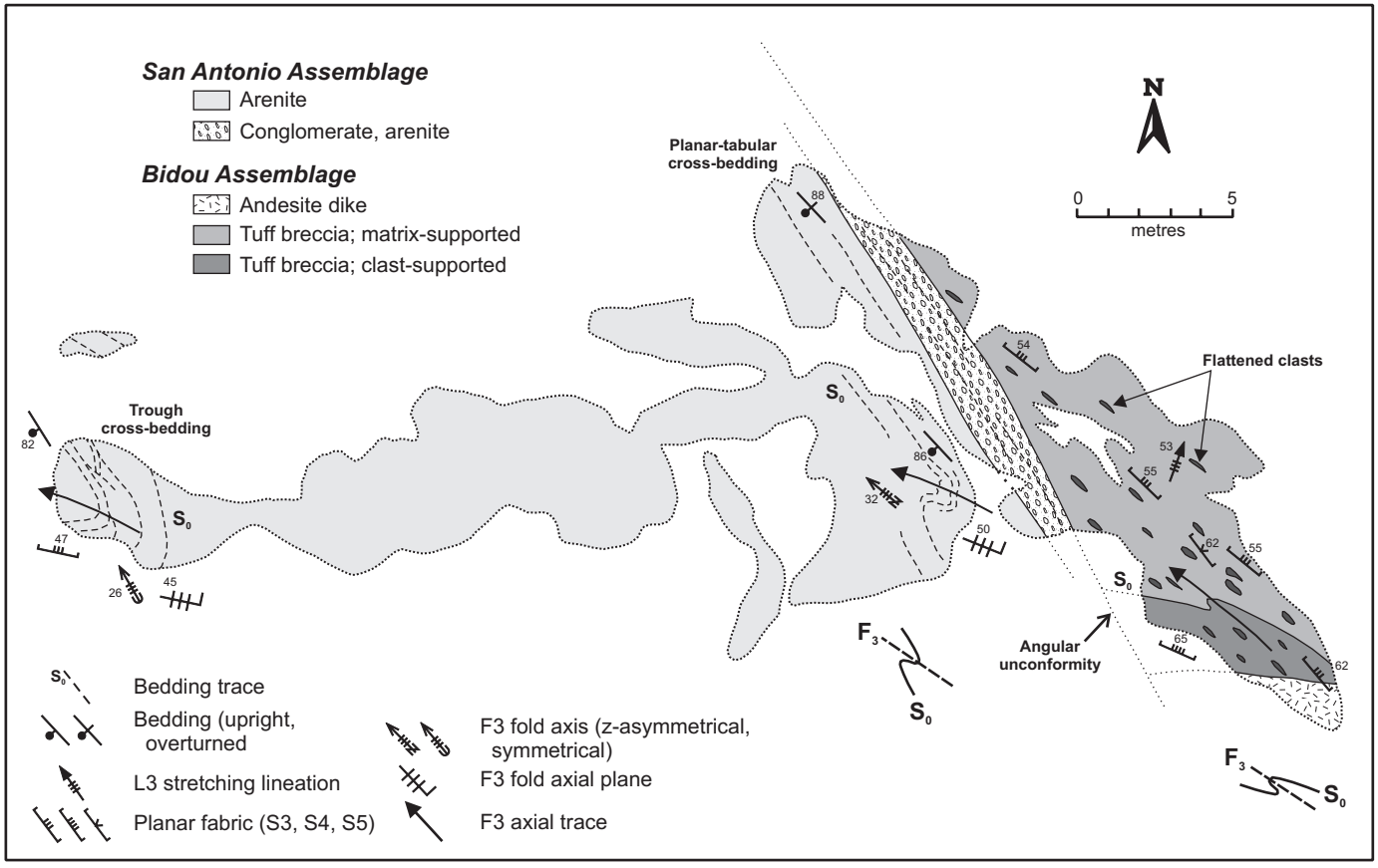
San Antonio Assemblage
Arenite
Conglomerate, arenite
Bidou Assemblage
Andesite dike
Tuff breccia; matrix-supported
Tuff breccia; clast-supported
N
0
5
metres
Planar-tabular cross-bedding
Trough cross-bedding
Flattened clasts
Angular unconformity
S_0
F_3
Bedding trace
Bedding (upright, overturned
L3 stretching lineation
Planar fabric (S3, S4, S5)
F3 fold axis (z-asymmetrical, symmetrical)
F3 fold axial plane
F3 axial trace

Figure 5

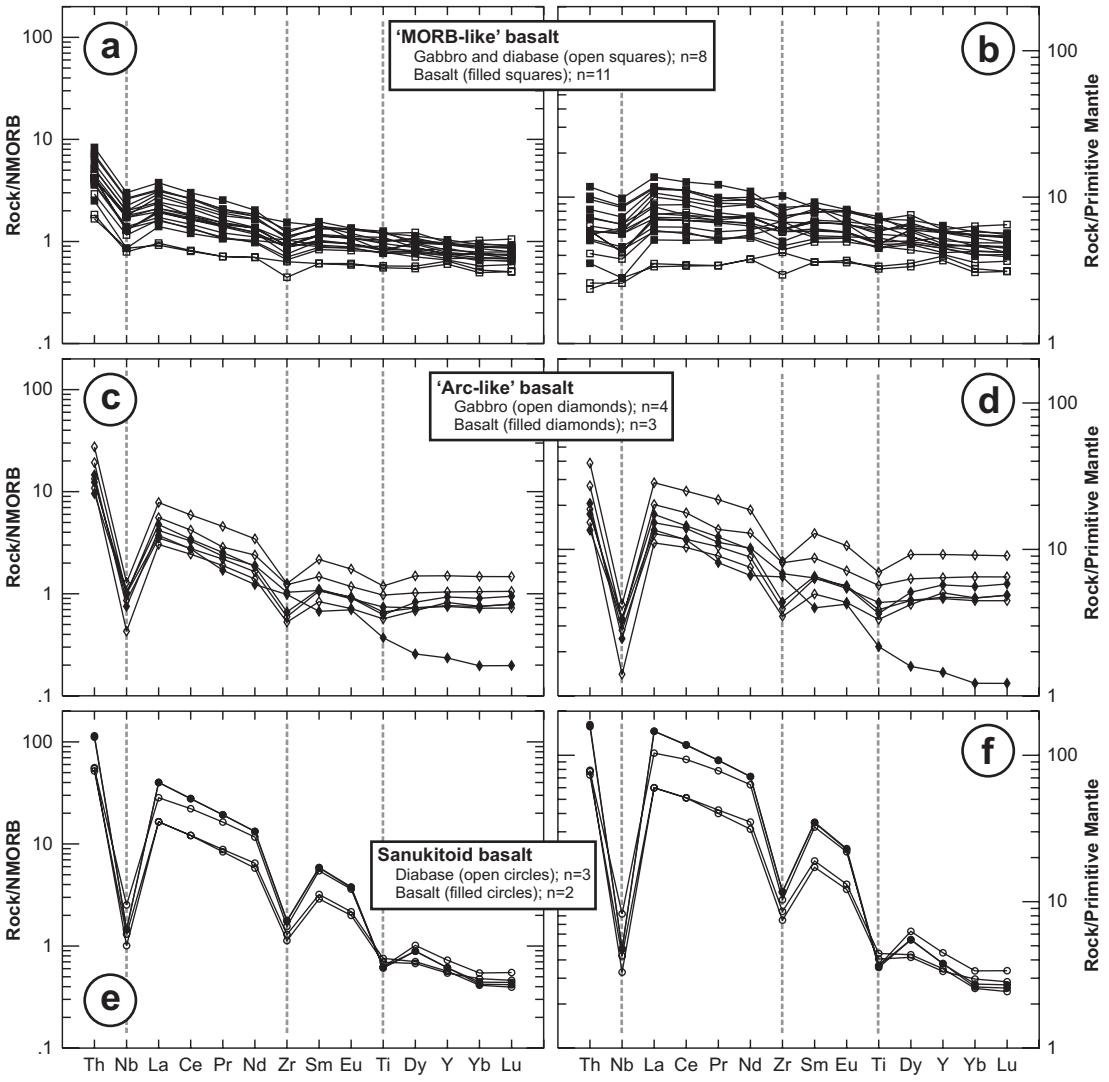
a
b
c
d
e
f
'MORB-like' basalt
Gabbro and diabase (open squares); n=8
Basalt (filled squares); n=11
'Arc-like' basalt
Gabbro (open diamonds); n=4
Basalt (filled diamonds); n=3
Sanukitoid basalt
Diabase (open circles); n=3
Basalt (filled circles); n=2
Rock/NMORB
Rock/Primitive Mantle
100
10
1
.1
Th Nb La Ce Pr Nd Zr Sm Eu Ti Dy Y Yb Lu

Figure 6

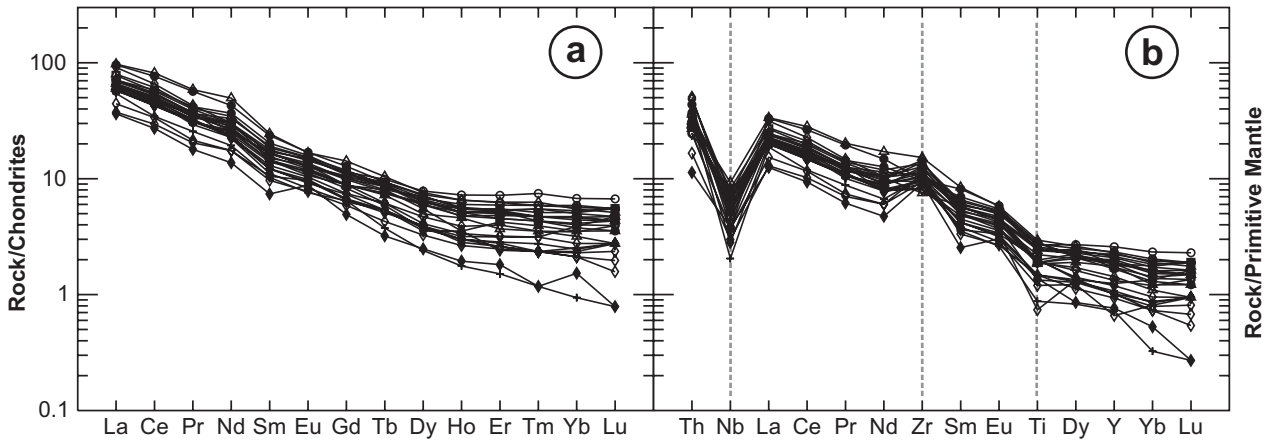
a
b
100
10
1
0.1
Rock/Chondrites
Rock/Primitive Mantle
La Ce Pr Nd Sm Eu Gd Tb Dy Ho Er Tm Yb Lu
Th Nb La Ce Pr Nd Zr Sm Eu Ti Dy Y Yb Lu

Figure 7

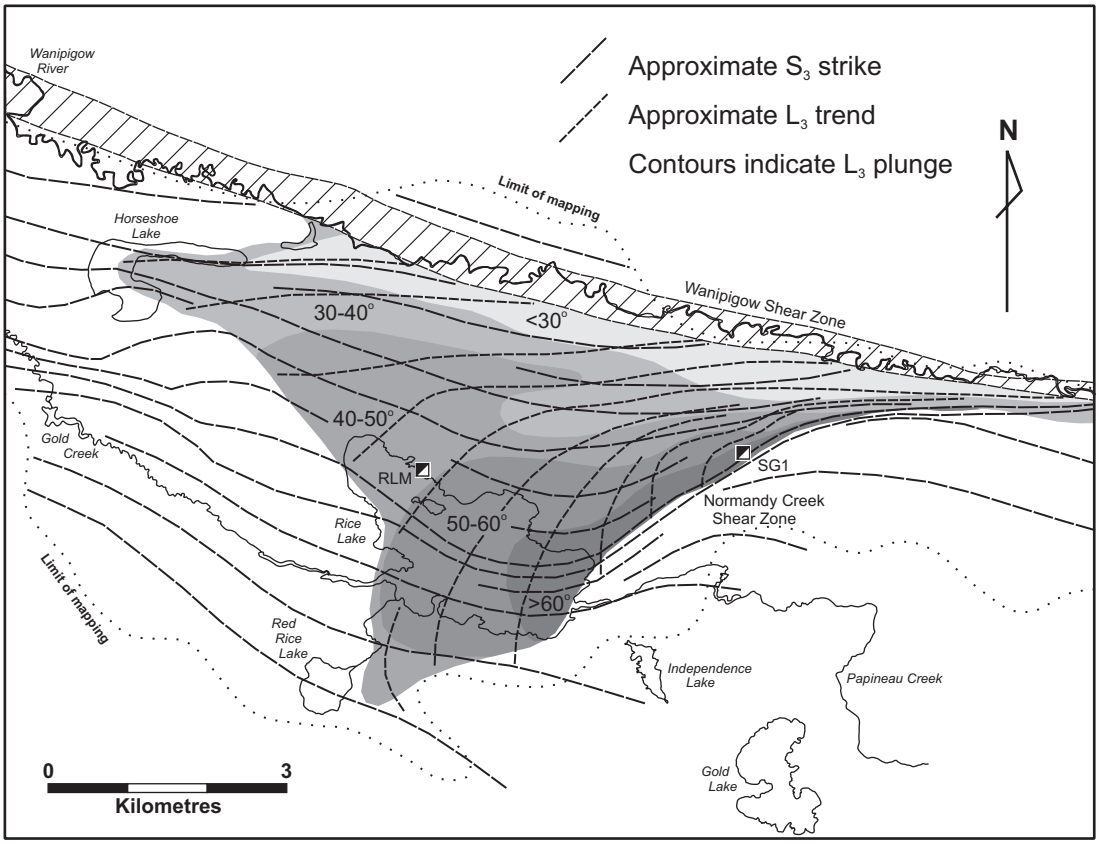
Wanipigow River
Approximate S_3 strike
Approximate L_3 trend
Contours indicate L_3 plunge
N
Limit of mapping
Horseshoe Lake
Wanipigow Shear Zone
30-40°
<30°
40-50°
Gold Creek
RLM
SG1
Normandy Creek Shear Zone
Rice Lake
50-60°
>60°
Limit of mapping
Red Rice Lake
Independence Lake
Papineau Creek
Gold Lake
0
3
Kilometres

Figure 8

D_2 Tilting, uplift and erosion (<2.715 Ga) of BA
Subsequent deposition of SAA (ca. 2.70 Ga)

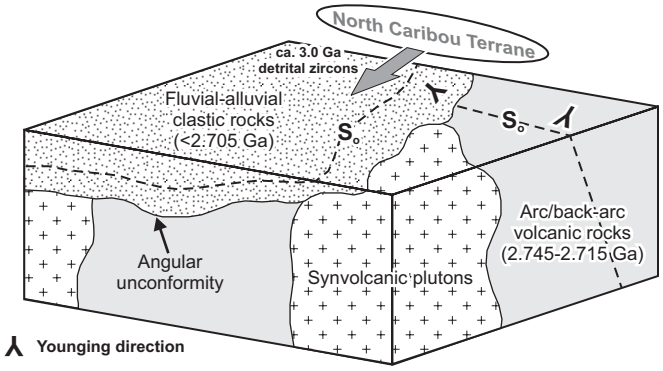

D_3 Basin inversion
Thrust faulting of BA over SAA
S-fabric adjacent to thrust fault

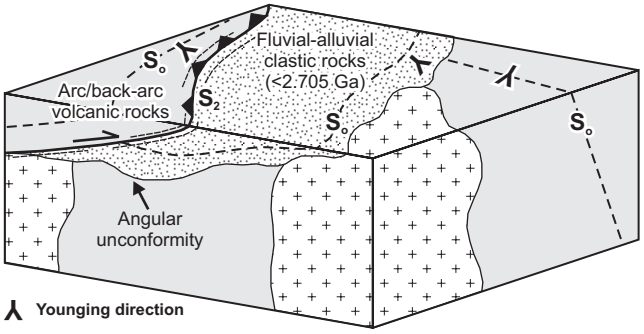

D_4 NNE-SSW shortening
Macroscopic folds in SAA
Penetrative S-L fabric in BA
Sinistral-reverse shear in WSZ

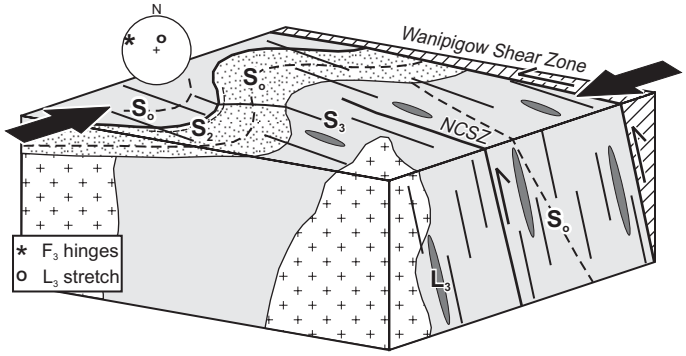

D_5 (early) NW-SE shortening
Penetrative cleavage
Dextral shear in WSZ & NCSZ(?)

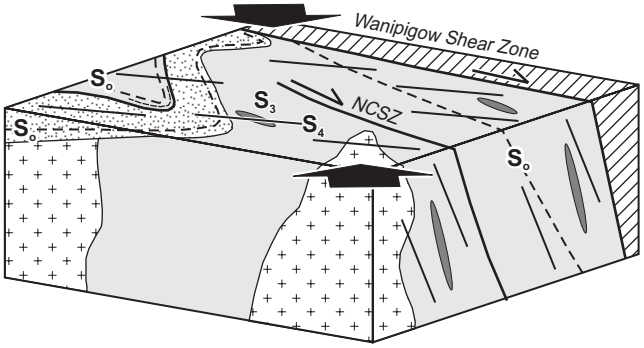

D_5 (main) NNW-SSE shortening
Main-stage dextral shear in WSZ
Regional spaced cleavage; high-strain zones
Re-orientation of F_3 and L_3 linear fabrics

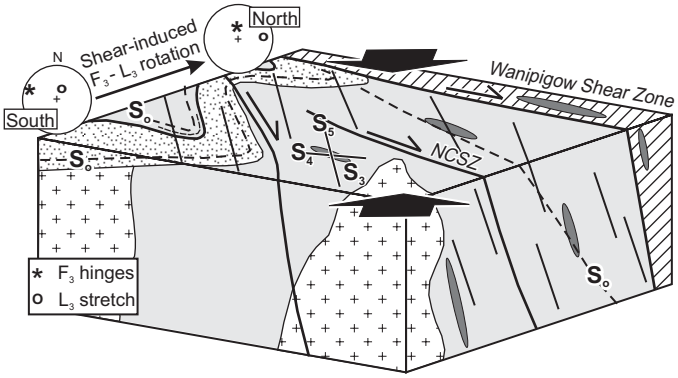

D_5 (late) Far-field NNW-SSE shortening
Continued dextral shear in WSZ
Local E-W shortening (buttress-effect on Ross River pluton)
Macroscopic folding (re-orientation of S_3-S_4-S_5 in NCSZ)

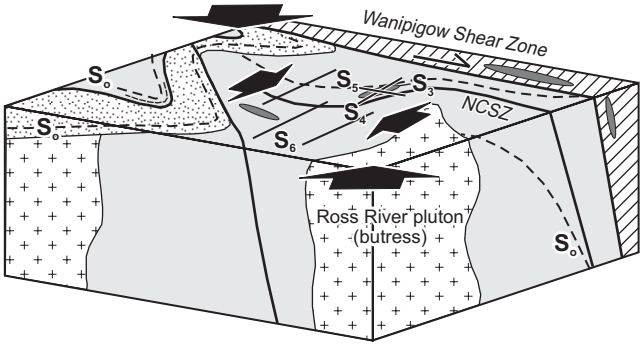

Figure 9

Table 1: Summary of ductile and ductile-brittle deformation in the Rice Lake area.

Generation	Shortening direction[a]	Mesoscopic structure	Macroscopic structure	Deformation episode and inferred tectonic significance
G_1	?	Penetrative to finely-spaced S_1 foliation in phyllite fragments in clastic dikes	Synvolcanic subsidence structures (normal faults)	D_1 : arc-extension; initiation of back-arc spreading?
	?	None observed	Early tilting of the Bidou assemblage	D_2 : arc-accretion and back-arc basin inversion?
G_2	?	Local, weak, layer-parallel S_2 foliation in San Antonio assemblage	Thrust fault at top of San Antonio assemblage	D_3 : basin inversion; continued accretion and/or initial crustal thickening
G_3	NNE-SSW	Regional WNW-trending S_3; steep L_3 stretching lineation; upright F_3 folds	Macroscopic folds (HLA, GCS); sinistral-reverse shear in WSZ	D_4 : collisional tectonics; crustal thickening
G_4	NW-SE	Regional, WSW-trending, S_4 crenulation cleavage; F_4 Z-folds		Early-D_5 : onset of terminal collision; dextral transpression
G_5	NNW-SSE	Regional S_5 shear-band cleavage; mylonitic S_5 in NW-trending high-strain zones; shallow L_5 lineation; F_5 Z-folds	Main-stage dextral shear in WSZ and subsidiary zones; coaxial flattening in NCSZ	Main-D_5 : terminal collision; dextral transpression
G_6	E-W	Open, north-trending F_6 crenulations	Open fold in the Bidou assemblage at Rice Lake	Late-D_5 : buttress effect on Ross River pluton; continued dextral transpression

Abbreviations: GCS, Gold Creek syncline; HLA, Horseshoe Lake anticline; NCSZ, Normandy Creek shear zone; WSZ, Wanipigow shear zone

[a] inferred trend of far-field maximum principal stress axis, based on *present* orientation of associated fabric elements